# AN OVERVIEW OF SILICON NANOSYSTEMS: STRUCTURAL PROPERTIES AND TECHNOLOGICAL APPLICATIONS


**A Graduate Project**

**SUBMITTED TO GRADUATE SCHOOL OF ADDIS ABABA UNIVERSITY**

**SCIENCE FACULTY, PHYSICS DEPARTMENT**

**IN PARTIAL FULFILLMENT OF THE REQUIREMENTS FOR THE DEGREE OF MASTER OF SCIENCE IN PHYSICS**

**BY ZELALEM ALEMAYEHU**

**ADVISOR: Dr. S.K.GHOSHAL**

**Addis Ababa**
**Ethiopia**

**March 2010**

**ADDIS ABABA UNIVERSITY**

**SCHOOL OF GRADUATE STUDIES**

# AN OVERVIEW OF SILICON NANOSYSTEMS: STRUCTURAL PROPERTIES AND TECHNOLOGICAL APPLICATIONS

BY

**ZELALEM ALEMAYEHU ANJULO**

**Department of Physics**

**Faculty of Science**

**Approved by the Examination Committee**

| Name | Signature |
|---|---|
| Dr. S. K. Ghoshal, Advisor | ---------- |
| | ---------- |
| | ---------- |

# Table of Contents

**Table of Contents** 3

**List of Figures** 5

**Abstract** 9

**Acknowledgements** 10

**1 Introduction** 11

1.1 Why silicon?. . . . .. . .. . . .. . .. .. .. . . . .. .. .. . . .. . . .. . . .. . .. . . .. . . . .. . . . . 11

1.2 Low dimensional silicon .. . . . . .. .. . .. . . .. . .. . .. . . . . .15

1.3 What are silicon nanocrystals? .. .. . . . .. . . . . . .. . .. . .. . . . .. . . .. . .. .. .. . . . . .17

1.4 properties of silicon nanocrystals. . .. . . . .. . . . . .. . . . .. . . .. . . . . . .. . . .19

1.4.1 Optical property of silicon nanocrystals.. . .. . . . . . .. . . .. . . . . .. . .. . . . . . 19

1.4.2 Electrical property of silicon nanocrystals .. . . . .. . . . . .. . . .. . .. .. . . . .. . . . 21

1.4.3 Non linaer optical property .. . . . . . . . . . . . . . . . . . . . . . . . . . . . . . . . . . . . . . . .22

1.5 Light emission from silicon nanocrystals and quantem confinment effect . . . .. . . . . . 24

1.6 Quantem dot quantem wires and quantem wells . . . . . .. . .. . .. . . . . . 27

1.7 Photoluminescence . . . .. . . . . .. . . .. . . . . . .. .. . . . . .. .. . .. . . . . . 29

1.8 Density of state .. . . .. . .. . . . . .. . . .. .. .. .. . . .. .. . .. . . . .. . . . .. . . . . . .. . . . . . .31

**2 Fabrication synthesized and characterization of silicon nanocristals 33**

2.1 Fabrication of silicon nanocrystals .. . .. . . .. . . . . .. . . . . .. . . . . .. . . . . .. . . .33

2.1.1 Preparation of porous silicon .. .. . . .. . . .. . .. . . .. . .. . . . . .. . . . . .. . .34

2.1.2 Ion implanted silicon nanocrystals .. . .. . .. . .. . . . .. .. . . .. . . .. . . . .. .. .35

2.1.3 Plasma Enhanced Chemical Vapor Deposition(PECVD)-grown silicon nanocrystallites . . . . . .. . . .. . . . . . .. . . . . . .. . . . . . .. . . . . . .. . . .37

2.2 Characterization of silicon nanocrystals .. . . .. . . .. .. . . . . . .. . . . . . .. . .39

**3 Theory modelling and simulation of silicon nanocrystal 41**

3.1 The pseudio- potential-Density Functional Theory applied to nanostructures. . .. . .. . . .41

3.1.1 Constructing pseudo-potential . . . . . .. . . .. . . . . . .. . . . .42

3.2 Structure of silicon nanocrystal in a computational approach . .. . .. . . . . .. . . .. . . .. .47

3.3 Modelling of silicon nanocrystals embedded in a $SiO_2$ matrix . . . . . .49

3.4 Modeling Quantem dot . .. . . . . .. . . .. . .. . .. . . .. . .. . .. .. .. . . . . . 50

**4 Silicon nanocristals enabling silicon photonics 51**

4.1 Silicon photonics . . . . . .51

4.2 Silicon wave guide. . . . . .. . . . . .. . . . . 53

4.3 Silicon modulators. . . . . .53

4.4 Silicon laser . . . . . .. . . . . ..55

4.5 Silicon photo-detectors. . . . . .. . . . . 57

**5 Application of silicon nanocristals for light emitting devices memory devices and solar cells 60**

5.1 Light emtting devices based on Si-nanoclusters . . . . . .60

5.1.1 Enhancement of the efficiency of light emitting devices based on silicon nanoclusters by coupling with photonic cristal . . . .. . . . . . .. . . . . . .. .. . . . 62

5.2 Silicon nanocrystals for dot memory . . . . . .. . . . . .. .. . .. . . . . . .63

5.3 Silicon nanoclusters for solar cell . . . . . .. . . . . .. . . . . .. .. .. .. . . . .65

5.3.1 Using silicon nanostructures for the improvement of silicon solar cells' efficiency. . . . . .. .. . . . . .. . . . . .. . . . . .66

**6 Summary and future outlook 70**

6.1 Summary . . . . . .. . . . . .. . . . . .. . . . . .. . . . . .70

6.2 Future outlook . . . . . .. . . . . .. . . . . .... . . . . .. . . . . .. .. . . . . .. ... . 71

**Bibliography 73**

# List of Figures

**1.1:** Diamond crystal structure for elemental silicon[13] . . . . . ..12

**1.2:** Silicon crystal[12] . .. . . . . .. . . . . .. . . . . 13

**1.3:** a) Brillouin zone for the diamond lattice, and b) bulk band structure of Si. The arrow in b) indicate the energies of the direct (1) and indirect phonon assisted transitions X (2) and L (3) →Γ→Γ [57] . . . . . 15

**1.4:** The transition energy is calculated for the; lowest electron and heavy hole energies for infnite confning potential (Left) [1]. . . . . ..16

**1.5:** a) A silicon nanocrystal (Si) embedded in a thin layer of silicon dioxide b) Silicon nanocristal embedded in $SiO_2$ [58] . . . . . .17

**1.6**: Silicon QDs as sensitizers for Erbium: high absorption cross-section of silicon nanocrystallites, their larger bandgap than corresponding interlevel spacing in $Er^{3+}$, and lower energy back transfer rate due to spatial decoupling are the main advantages of such a mechanism of Erbium excitation [56]. . . . . .18

**1.7:** Upper part: PL spectra of PSi samples having different nanocrystal size distributions. Lower part: spectral dispersion of singlet exciton lifetime. $T$=200K. $E_{ex}$=3.67 eV . . . . . .20

**1.8:** Typical static I–V characteristics of a 10 min-RTO diode sample thickness of 10 nm) measured at room temp. where the measurements delay time is 60 s[59]. . . . . .21

**1.9:** Typical dynamic I–V characteristics of (initial a–Si: H 10 min (solid curve) and 30 s (dashed curve) RTO diode sample (initial a–Si: H thickness of 10 nm) measured at room temp., where the measurement delay time is 0 s[59]. . . . . .21

**1.10:** Time dependence of the tunnel current (100 ms to 100 s) for the 10 min-RTO diode sample with the gate voltage as a parameter. The measurement was performed at room temperature [60]. with Si-nc radius. Dashed lines are a theoretical [61]. . . . . 22

**1.11:** Variation of χ (3) with Si-nc radius (r) in Si-nc grown by PECVD. Inset shows the PL peak maxima variation nanocrystallites [26]. . . . . 24

**1.12:** The increase of the band gap with decreasing crystalline size due to quantum confinement [62] . . . . . .27

**1.13:** a) Schematic evolution of the electronic structure between the macroscopic solid and nanocrystal of decreasing size. b) Theoretical variation of the gap calculated from the equation for the nanocrystals of different semiconductors [63] . . . . . 27
**1.14:** Schematic of low dimensional Structure[64] . . . . . 28
**1.15:** Photoluminescence peak energy of silicon nanocrystallites as a function of crystal size. The solid line was obtained from the effective mass theory for three dimensionally confined Silicon. . . . . 30
**1.16**: Room-temperature photoluminescence spectra of silicon nanocrystallites. The peak position can be controlled by appropriate adjustment of the nanocrystallitesize [26]. . . . . .31
**1.17:** Density of states for various geometries of semiconductor materials: (a) 3-D bulk, (b) quantum well, a 2-D structure, (c) quantum wire, a 1-D structure, and (d) quantum dot, a 0-D entity. The dotted line in (a) is the thermal distribution of carriers [63] . . . . . 32

**2.1:** silicon nanocrystal fabrication techniques[64]. . . . . .34
**2.2:** Formation of porous silicon. (Left) SEM image illustrating the three typical etching regimes in silicon: porous formation, transition regime with pillar-like structures, and electropolishing[25]. (Right) TEM micrograph of porous silicon grains with characteristic size of several nanometers [40] . . . . . 35

**2.3:** Formation of silicon nanocrystallites in a $SiO_2$ shell by implantation of silicon ions of 270keV energy into silicon dioxide with subsequent annealing [25]. . . . . 36
**2.4:** Synthesis of Si by ion implantation method[67]. . . . . 37
**2.5a)** scheme of the PECVD aparatus for the Deposition process[68] . . . . . 38
**2.5b)** state of preparetion of silicon[68] . . . . . 38
**2.6a)** AFM image of Si-nc on the basal plane of HOPG formed by evaporation of at 17000in argon buffer gas. **b)** The size distribution of the Si-nc determined from the AFM height mode[69] . . . . . 39
**2.7 a)** HRTEM micrograph of Si-nc in $SiO_2$.Implant condition; 100KeV Si-; corresponding to an excess Si conc. of 10at. % at projected range of150nm Annealed 1100c; 16hr **b)** Size distribution of Si-nc[70]. . . . . .40

**3.1:** Standard pseudo-potential of a solid[71]. . . . . 42

**3.2:** Uniform grids illustrating a typical configuration for examining the electron structure of a localized system. The gray sphere represents the domain where the wave functions are allowed to be non-zero. The light spheres within the domain are atoms [72] . . . . . 46

**3.3:** Ground state geometries and some low-energy isomers $Si_n$ ($n \leq 7$) clusters[34]. . . . . ..48

**3.4:** Binding energy of $Si_7$ during a Langevein simulation[73]. . . . . 48

**3.5:** The optical gain spectrum for the $Si_{10}$ nanocluster embedded in a $SiO_2$ matrix in the low energy region. . . . . 49

**3.6:** Atomic structure of a Si quantum dot with composition $Si_{525}H_{276}$ [74] . . . . . 50

**4.1:** Intel's vision of an integrated silicon phonics chip[75] . . . . . .51

**4.2:**The building blocks of the integrated optical circuit[75] . . . . . 52

**4.3:**Schematic of a Mach-Zender interferometer modulator with two phase shifter sections[75]. . . . . .54

**4.4:** Top-down schematic of Intel's silicon laser[75] . . . . . ..55

**4.5:**Silicon Laser used in Intel's experiments[75] . . . . . .56

**4.6:**SEM image of Intel's Silicon Laser[75] . . . . . .56

**4.7:**Absorption coefficient and penetration depth of various materials as a function of λ. Green lines mark important communications wavelengths of 1.31μm and 1.55μm [75]. . . . . ..58

**4.8:** SiGe waveguide-based photo-detector on a SOI wafer[75] . . . . . ..59

**5.1:** (a) EMMI image of a device with 46 at.% Si annealed at 1100°C for 1 h. The colors indicate different intensities of the emitted light, red being the highest. (b)Comparison between the PL and the EL spectra of a device with a Si content of 42 at.% in the SiOx layer. The EL spectrum was measured with a voltage of −48 V and a current density of 4 $mA/cm^2$. . . . . 61

**5.2:** (a) EL spectra for the unpatterned, random, and photonic crystal devices. An EL intensity enhancement accounting for a factor of 4 at 860 nm is demonstrated in the photonic crystal device. (b) Polar distribution of the emitted radiation at a wavelength of 860 nm. Tilt is along GM direction. . . . . .63

**5.3:** Time dependence of the stored-charge from the flat-band state, after electrons were injected in floating-gates, shows a logarithmic discharging behavior. The gate voltage was kept at the initial flat-band voltage: -1.6V for sample A (surface nitrided nc-Si dots) and -2.4V for sample B (without nitridation). The inset shows the structure of memory device . . . . . 64

**5.4:** Energy loss processes in a solar cell schematically depicted. The zone denoted by A represents the low-energy photon losses resulting from the material band gap, whereas the zone denoted by B represents the high-energy photon losses resulting from phonon scattering (thermalization). . . . . .67

**5.5:** Comparison of PL spectra between porous silicon, SiNx and SiOx samples. The PL intensity of SiNx and SiOx samples is equivalent but still a factor 100 below that of porous silicon sample [76]. . . . . ..67 **5.6:.** PL spectrum obtained from SiNx= samples for 0.5<x <1.1 showing the energy dependence of the emission on silicon content[76]. . . . . .68

**5.7.** HRTEM image of nanocrystalline Si precipitates embedded in a UVassisted silicon-rich (x =1.1) nitride film: (a) observation of the Si precipitates on a large scale with a density of $1.5\_10^{12}$ $cm^{-2}$; (b) zoom image showing the shape and length of few Si nanocrystals; and (c) ring patterns for the transmission electron diffraction from the Si nanoprecipitates showing their crystalline nature [76]. . . . . 68

**5.8:** PL dependence on annealing duration under $O_2$ atmosphere for SiOx=1.5 samples. An increase of annealing temperature reduces the nanoparticle size producing an increase of the optical band gap and a blue shift of the PL energy. Inset: Typical TEM image showing the silicon nanostructures formed after high temperature annealing [76]. . . . . .69

# Abstract

Low dimensional nanosystems are known to have properties that can be markedly different from their bulk counterparts. For semiconductor crystals such as silicon when the carriers (excitons) are confined in dimensions less than their de Broglie wavelength (typically a few nanometers) quantum mechanical size effects emerge.

Advances in the design, synthesis and characterization of nano-materials are expected to provide the unprecedented ability to manipulate matter at the most fundamental level. When the physical dimensions of a device are reduced to the nanometer scale, quantum phenomena become prevalent modifying the optical and electronic properties of the material. This may enable the design and manufacturing of materials with properties tailored for the particular application.

This paper examines the unique properties of silicon-based nanocristals that are fundamentally different from those of the bulk crystalline material and make nanoscale silicon attractive for use in a variety of important technological applications such as light emitting devices for potonic application,optical communications, photovoltaic solar cells,for memory devices, optical and electrical properties of nanoscale silicon and several techniques towards developing silicon-based nanostructures using nanotechnology tools are explored.

Moreover, the different synthesis methods of silicon nanostructures and the accompanying characterizations of silicon nanocrystals and porous silicon are illustrated briefly. Theoretical analysis of the electronic structures of silicon nanocrystals of small number of atoms using pseudo potential-DFT method is presented.

In general, for the last fiften years so many researches and jornals are published on silicon nanosystems,in this work we try to give an overview of the applications properties and dimond cristal structure of elemental silicon.

# Acknowledgements

I would like to thank my advisor, Dr. S.B.Ghoshal for his many suggestions and constant support during this paper. I also thank him for his guidance and for supportive materials he has been providing since I joined him. He gave me invaluable guidance, advice and constructive comments.

I am very grateful to my God, my mother Amarech, my father Alemayehu, my sisters Selamawit and Weineshet and, my brothers Tesfahun and Antehun for their patience and love.

# Chapter 1

# Introduction

In this chapter we are going to see why silicon,low dimensional silicon, silicon nanocristals, optical properties of silicon nanocristals,photoluminescence,light emission from silicon nanocristal,quantem confinement effect and finally we will see density of state. All these enable as to overview of the paper

## Objectives

### General Objectives

- To understand the structure of silicon nanosystems.
- To understand the properties of silicon nanosystems.
- To applicate silicon nanosystems for devices for solar cell and for photonics.

### Specific objectives

• To describe silicon nanosystem.
• To understand how synthesized, fabricated and characterized of silicon nanosystem.
• To describe quantem confinment effect of silicon nanocristal.
• To distingush the enahancement of silicon nanosystem for applications.
• To explain silicon nanophotonics.

## 1.1 Why Silicon?

Silicon (Si) is the chemical element in the periodic table with atomic number 14 .Its standard state is solid at 298K.It is the second most abundant element next to oxygen in the earth's crust in nature. It occurs most often as oxides and as silicates. Sand, amethyst, agate, quartz, rock crystal, fling, jasper, and opal are some of the forms in which the oxide appears. Granite, asbestos, feldspar, clay, hornblende and mica are a few of the many silicate minerals similar to

other group IV elements [11]. Silicon easily forms four covalent σ bonds in tetragonal coordination ($sp^3$ hybridization) and typically crystallizes in a diamond like structure.

**Production of bulk silicon:** Silicon is commercially prepared by the heating of high purity silica in an electric arc furnace using carbon electrodes [12]. At temperatures over $1900\ ^0c$, the carbon reduces the silica to silicon according to the chemical equation:

**Isolation:** there is normally no need to make silicon in the laboratory as it is readily available commercially. Silicon is readily available through the treatment of silica, $SiO_2$, with pure graphite (as coke) in an electric furnace.

$$SiO_2 + 2CSi \rightarrow Si + 2CO \qquad (1.1.1)$$

Under these conditions, silicon carbide, SiC, can form. However, provided the amount of $SiO_2$ is kept high, silicon carbide may be eliminated.

$$2SiC + SiO_2 \rightarrow 3Si + 2CO \qquad (1.1.2)$$

**Characteristics and Structure of bulk silicon: -** This crystalline form silicon has a metallic luster and a grayish color. Even though it is a relatively inert element, silicon still reacts with halogens & dilute alkalis, but most acids (except for a combination of nitric acid and hydrofluoric acid) do not affect it [11]. Silicon is a semiconductor with a diamond lattice structure. Due to its unique electrical properties, it is the most important technological material in electronics industry. The crystal structure of crystalline silicon is illustrated in figure 1.1 [13].

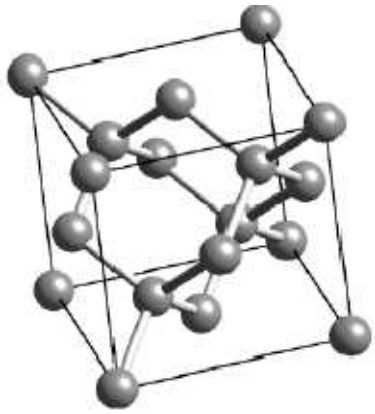

Figure 1.1 Diamond crystal structure for elemental silicon [13].

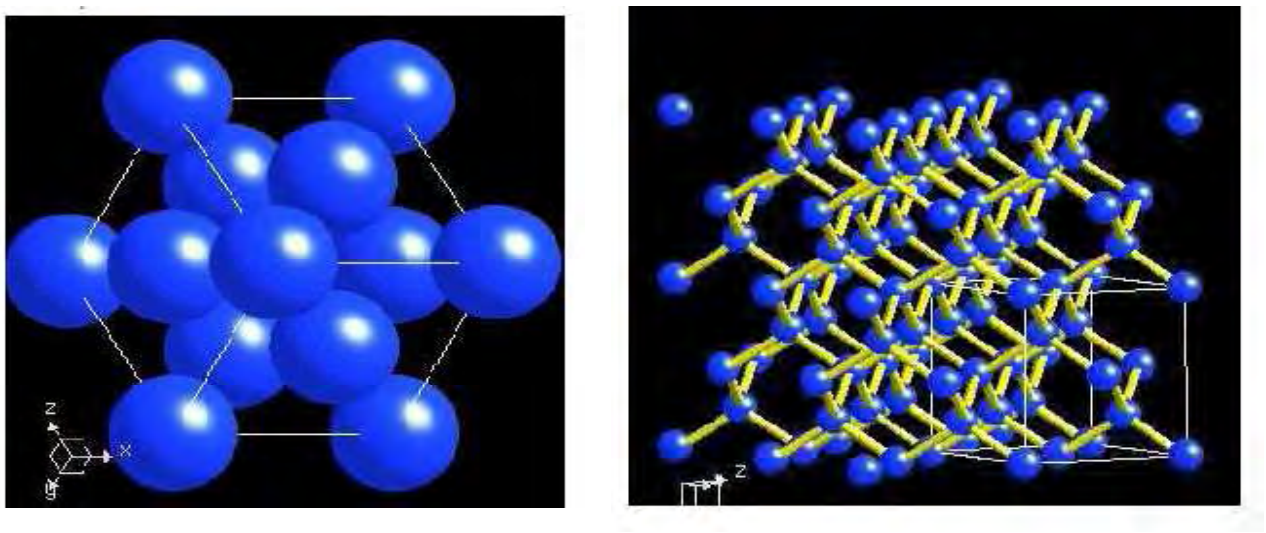

**Fig 1.2:** silicon cristal[12].

Semiconductor devices are key components in modern electronic systems. Silicon and gallium arsenide with its related III-V compounds form the basis of the most commonly used semiconductor materials. However, silicon is by far the major player in today's electronics market, dominating the microelectronics industry with about 90% of all semiconductor devices sold worldwide being silicon based. But why is silicon still the most important semiconductor material, Its dominance is mostly due to the following aspects, which provide benefits that other electronic materials cannot easily match:

- Silicon possesses two of the most outstanding natural dielectrics, silicon dioxide ($SiO_2$) and silicon nitride ($Si_2N_2$), which are essential for device formation. In particular, $SiO_2$, which is the basis of the metal – oxide – semiconductor devices (MOS) can be grown thermally on a silicon wafer, it is chemically very stable and can achieve a very high breakdown voltage. The interface defects of the thermally grown $SiO_2$ by reaction of oxygen with a silicon wafer are several orders of magnitude lower than those of any deposited film.

- Silicon is non-toxic, relatively inexpensive (silicon comprises about 26% of the earth's crust which makes it second in abundance only to oxygen), easy to process (a very well established industrial infrastructure in silicon processing exists around the world), and has quite good mechanical properties (strength, hardness, thermal conductivity, etc.).

For all the above reasons, silicon is the cornerstone material in electronic systems. However, one of the most important limitations of bulk silicon is in optoelectronic applications, because of its inefficiency at emitting light. This is due to its indirect fundamental energy band gap, which essentially makes optical transitions in the bulk material at room temperature a very rare phenomenon. In a semiconductor with an indirect fundamental energy band gap, the maximum of the valence band and the minimum of the conduction band are found at different locations in the k-space. Recombination by a single photon – which carries negligible momentum – is not allowed, because of momentum conservation. Participation of a phonon with the right momentum is necessary to satisfy momentum conservation. Phonons are quantized modes of lattice vibrations that occur in a solid. In the bulk material, this phonon assisted optical transition is very weak, allowing many other non-radiative processes to dominate resulting in a huge drop in the light emission efficiency.

Bulk silicon is therefore not suitable for the implementation of optoelectronic devices. To date, the semiconductor optoelectronics industry has been dominated by the III-V compound semiconductors, because of their high efficiency in optical transitions primarily due to their direct fundamental energy band-gap. As a consequence of its indirect band gap, bulk silicon has a typical room temperature quantum efficiency of < 0.001% compared to around 1-10% for GaAs LEDS and around 30% for specialized GaAs and InP devices [14]. This poor efficiency results primarily from the fact that the lowest energy transition (figure1.3b) violates conservation of momentum and therefore requires phonon assistance. Consequently, the exciton lifetime is very long and non-radiative recombination dominates the relaxation process. In nanoscale structures, the requirement for momentum conservation is relaxed and the probability for direct transmission is increased.

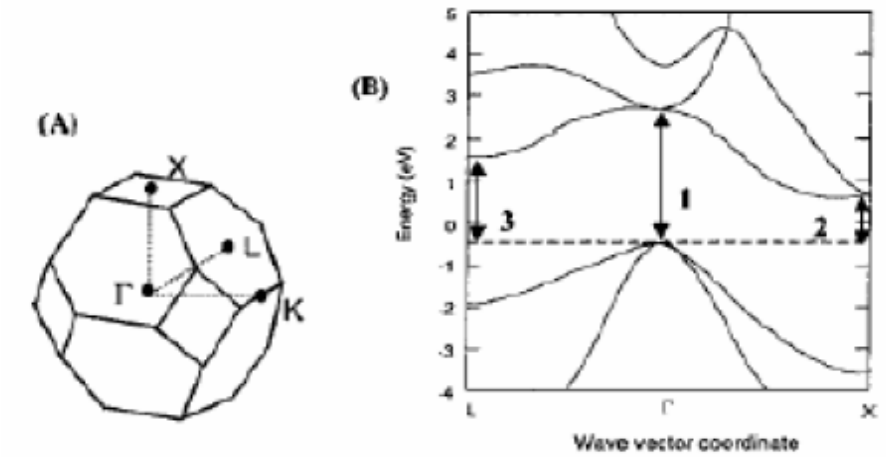


Figure 1.3 a) Brillouin zone for the diamond lattice, and b) bulk band structure of Si.
The arrow in b) indicate the energies of the direct (1) and indirect phonon assisted transitions X (2) and L (3). →Γ→Γ[57].

## 1.2 Low Dimensional Silicon

As we change the dimensionality of Si very fascinating and new optical properties of the material appear, light emission starts to be a very efficient process in nanostructured Si and light emitting diodes with effciency in excess of 1% have been fabricated [1]. Optical amplification has been also observed when Silicon nanocrystals are embedded into a dielectric matrix, such as $SiO_2$. This makes the Si in a dielectric matrix system a potential candidate for laser action. In addition to electronic property variations, nanostructured Si can also be used as nanodielectric material, where controlled changes in a refractive index can lead to trapping or slowdown of photons. In this and in the following sections we aim to give the explanation of low dimensional Si both its electronic and its dielectric properties. The best way to understand the effects of the reduced dimensionality on the energy spectrum of an electron is to resort the particle in-a-box problem so familiar in quantum mechanics. Within the effective mass approximation in the envelope wave function description, the transition energy of an electron-hole pair of effective reduced mass μ confined in a quantum dot modeled as cubic box of sides $L_x$, $L_y$, and $L_z$ is given by

$$E_{e,h} = E_g + \frac{\hbar^2}{2\mu}\left[\left(\frac{n_x}{L_x}\pi\right)^2 + \left(\frac{n_y}{L_y}\pi\right)^2 + \left(\frac{n_z}{L_z}\pi\right)^2\right] \quad (1.2.1)$$

Where we have assumed that the cofined energy barrier is of infinite strength and that $E_g$ is the energy band gap of the bulk semiconductor, (i.e Silicon), $n_x$, $n_y$ and $n_z$, are the quantum numbers to describe a given quantized energy level. Equation shows that the effective energy band gap of the Silicon quantum dot increases as the quantum dot dimension decreases. If we assume the dot to be spherical, we have

$$E_{e,h} = E_g + \frac{\hbar^2}{2\mu}\left(\frac{n\pi}{d}\right)^2 \quad (1.2.2)$$

Where d in the equation is the diameter of the dot. The transition energy scales with $1/d^2$ law. More accurate calculations show that the scaling law doesn't follow an exact power 2 law but instead the exponent is lower [1]. A value of 1.7-1.8 seems to be more appropriate. The transition energy and optical energy gap in quantum dot, quantum wires and quantum wells increases as their size decreases.

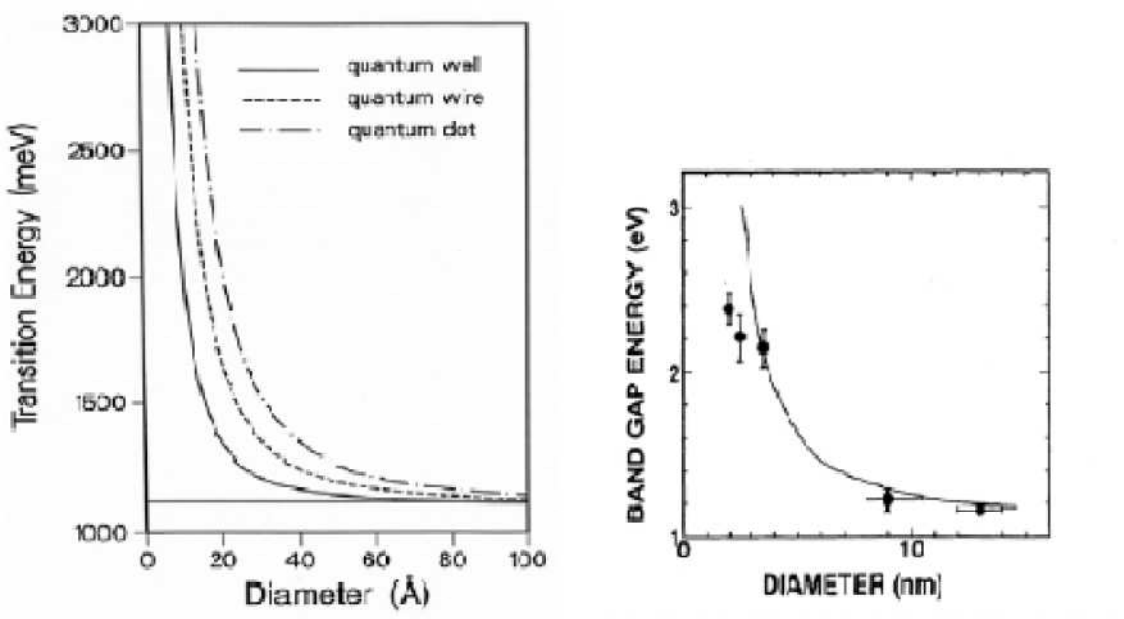


**Figure 1.4:** The transition energy is calculated for the; lowest electron and heavy hole energies for infnite confning potential (Left) [1].

The assumption of having an infinite potential barrier is very crude since silicon nanocrystals (Si-ncs) are usually formed in a dielectric matrix usually a silica glass ($SiO_2$) but more recently the use of $Al_2O_3$; $Si_3N_4$ or oxynitride is emerging as an alternative [1]. Also the effective mass approximation has strong limitation since the reconstruction of the lattice in the dots caused by the strain and elastic properties of the host should be considered. Finally, chemical bonds among the surface Si atoms of the Si-nc and the atoms of the host strongly modify the energy spectrum of Si-nc.

## 1.3 What are silicon nanocrystals?

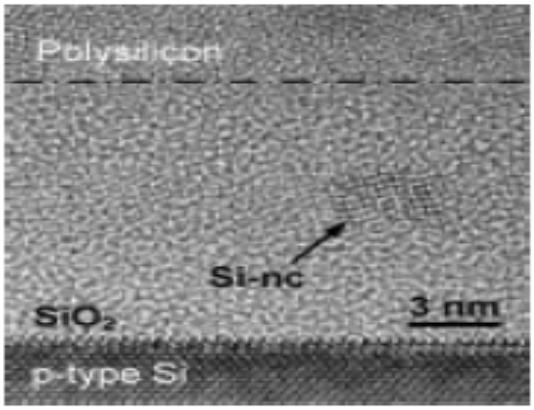


Fig 1.5a)

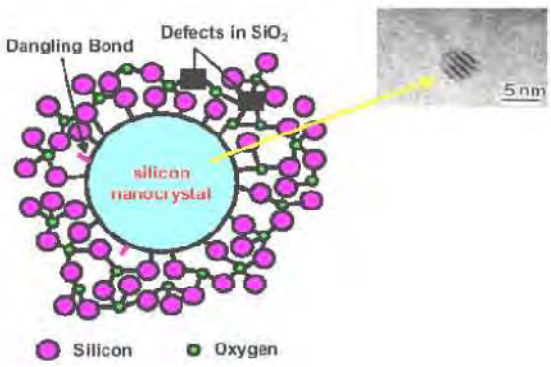


Fig 1.5b)

1.5a) A silicon nanocrystal (Si) embedded in athin layer of silicon dioxide b) Silicon nanocristal embedded in $SiO_2$[58].

A nanocrystal is a single crystal having diameter of a few nanometers. Silicon/silicon dioxide, ($Si/SiO_2$) nanocrystalline quantum dots are silicon clusters, completely embedded in silicon dioxide . The Si nanocrystals in the Si-related nanoparticles are ideal quantum dots with a stable surface, where carriers (electrons and holes) and phonons are to be confined. The physical properties unique to silicon quantum dots make Si more attractive as a material of optoelectronic and functional devices. The sizes of Si quantum dots can be precisely controlled by their interaction with coherent light causing so-called photo-oxidation.

Integration and economy of scale are the two key ingredients in the technological success of silicon. Its band gap (1.12eV) is ideal for room temperature operation, and its oxide ($SiO_2$) allows the processing flexibility to place more than $10^8$ transistors on a single chip. The continuous improvements in silicon technology have made it possible to grow and process 300mm wide single silicon crystal at low cost and even larger crystallites are now under development.

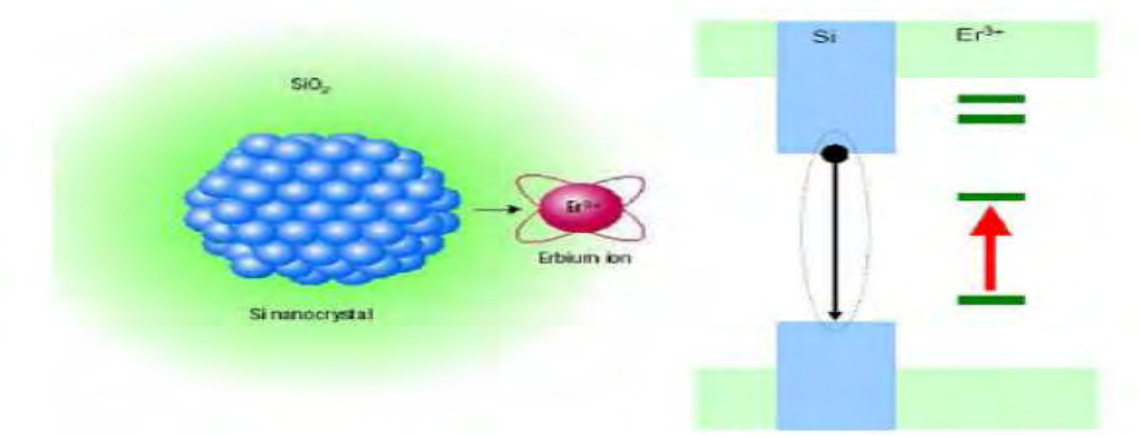


**Figure1.6**: Silicon QDs as sensitizers for Erbium: high absorption cross-section of silicon nanocrystallites, their larger bandgap than corresponding interlevel spacing in $Er^{3+}$, and lower energy back transfer rate due to spatial decoupling are the main advantages of such a mechanism of Erbium excitation [56].

In this chapter we will discuss the different properties of silicon nanocrystals and in the next chapter we will see the different synthesis methods.

# 1.4 properties of Si nanocrystals

## 1.4.1 *Optical properties of Si nanocrystals*

Bulk Si is very inefficient light emitter due to very small oscillator strength of optical transitions and efficient capture of excitons or *e-h* pairs to nonradiative centers or doping impurities. In a nanocrystal, the situation changes. Firstly, spatial confinement according to the prediction of quantum confinement model has to shift both absorbing and luminescing states of nanocrystals to higher energies due to a rising of the minimum allowed kinetic energy of confined charge carriers. Secondly, according to the uncertainty principle, the geometrical confinement leads to a delocalization of carriers in the crystal quasi momentum space thus allowing zero phonon optical transitions.[40,43,44] Thirdly, due to the better overlap of electron and hole envelope wave functions one can expect a strong enhancement of the oscillator strength of optical transitions and of the *e-h* exchange interaction inducing a splitting of the exciton levels.[40,45]

Finally, since photoexcited carriers are strongly geometrically localized in nanocrystals they were created, recombination has the geminate character. Therefore the recombination statistics for Si nanocrystals assemblies is quite different from that used for bulk crystals. Measured PL lifetimes can be considered to a large extent to be radiative. This can be understood by regarding Si nanocrystal assemblies as a granular-like materials consisting of luminescing (internal quantum yield is equal to 1) and dark nanocrystals. Crystallites of the first type belong to those which do not contain nonradiative centers while the second ones have at least one surface nonradiative defect. Under this assumption the observed PL decay time is the time of radiative recombination.[46,47]

Clear evidence that emitting states of different types of Si nanocrystals assemblies are driven to higher energies by the confinement is an observation that energy of PL maxima correlates very well with Si nanocrystal size distribution.[41,42] The PL, depending on the mean size of Si nanocrystals, can be continuously tuned with small increments over a very wide spectral range

from the Si band-gap to almost the green region. Despite PL measurements performed on individual Si nanocrystals have confirmed their atomic-like emission. [48]PL from assembles of Si nanocrystals is very broad due to residual nanocrystals size and shape. The study of the temporal PL behavior is very important since it allows the prediction of possible optical behavior under certain excitation conditions.

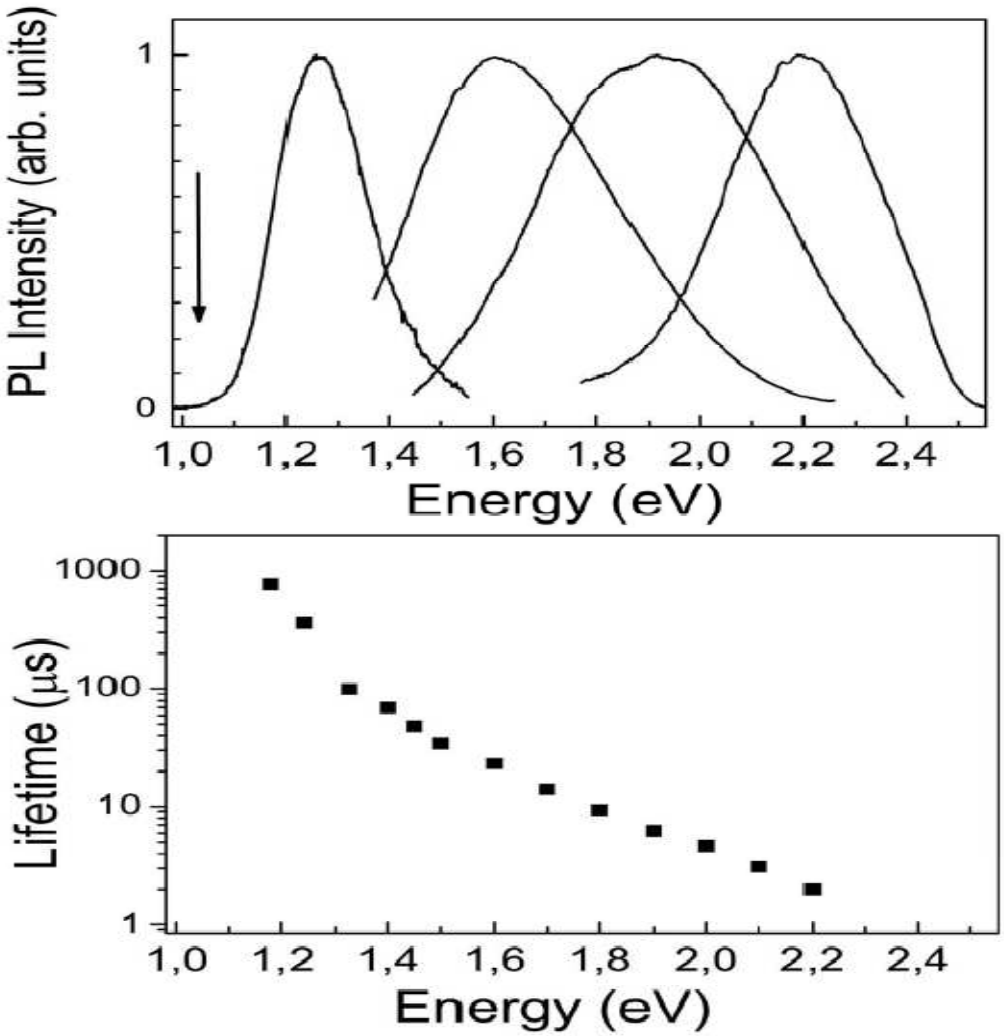


**Figure 1.7:** Upper part: PL spectra of PSi samples having different nanocrystal size distributions. Lower part: spectral dispersion of singlet exciton lifetime. $T$=200K. $E_{ex}$=3.67 eV.

## 1.4.2 Electrical property of silicon nanocristals

The electrical transport properties of Si-nc are determined mainly by its microstructures. With silicon nanocrystals embedded in ultra thin oxide by the rapid thermal oxidation (RTO) of an ultra thin chemical vapor deposition (CVD) amorphous Si (a-Si: H) film, some novel features such as the current peak and valley and the hystersis are revealed in I-V characteristics curve of the diode structure. This suggests the charging of a definite amount of electrons at the silicon nanocrystals and the subsequent screening effect on the tunnel current following the diode structure [16].

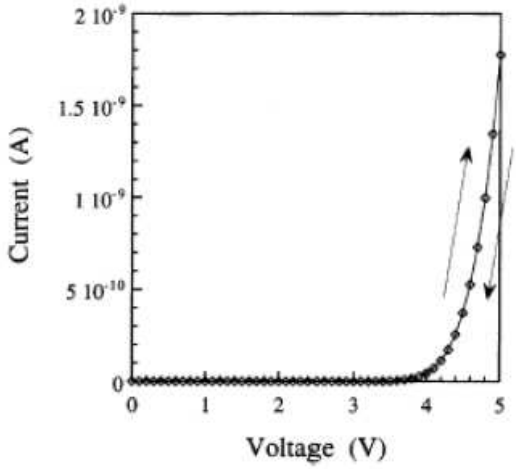


Fig 1.8

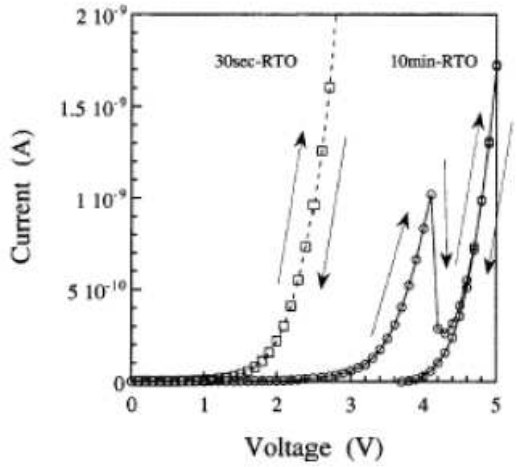


Fig 1.9

**Figure1.8:** Typical static I–V characteristics of a 10 min-RTO diode sample thickness of 10 nm measured at room temp. Where the measurements delay time is 60 s. [59].

**Figure 1.9:** Typical dynamic I–V characteristics of initial a–Si: H 10 min (solid curve) and 30 s (dashed curve) RTO diode sample (initial a–Si: H thickness of 10 nm) measured at room temp., where the measurement Delay time is 0 s.[59].

Figure 1.8 shows the typical round sweep I-V characteristics of a 10-min –RTO diode sample where the delay time is 60 second. The round sweep I-V characteristics measured under the delay time of 0 second for the same sample is represented in figure 1.9. It should be noted that the I-V characteristics measured under the minimum delay time reveal the novel features of the current peak and valley at the gate voltage from 2.5- 4.2V.in the forward sweep. In contrast, the

reverse sweep I-V curve, shows no current peak and valley in the forward sweeps is not attributed to the resonant tunneling. It is important to note that the formation of Si –nanocrystals of less than 5nm in size leads to these novel features. The exact electron trapping sites at the silicon nanocrystals are unknown at present. However, it is not considered that the electron stays in the conduction band of the silicon nanocrystal. The time dependence of the tunnel current for the 10 min-RTO diode samples is summarized in figure 1.10.

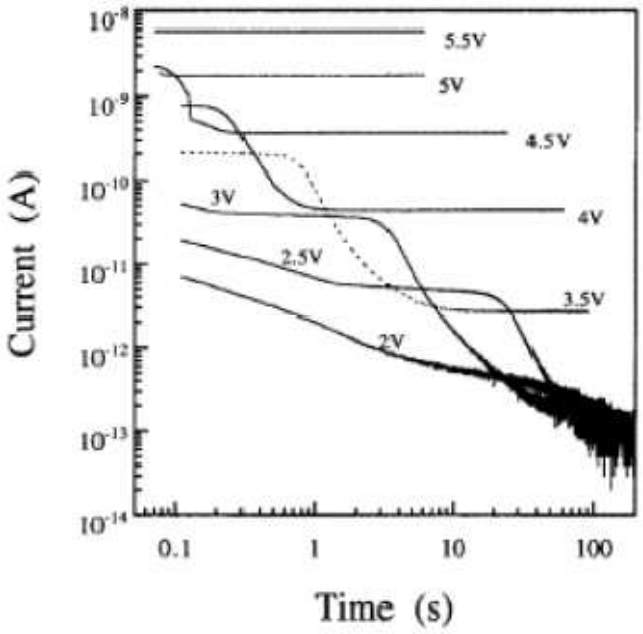


**Figure 1.10:** Time dependence of the tunnel current (100 ms to 100 s) for the 10 min-RTO diode sample with the gate voltage as a parameter. The measurement was performed at room temperature [61].

### 1.4.3 Non-linear Optical Properties

In typical semiconductor nanocrystals, energy level spacing is in the order of about 0.2eV, depending on the material and quantum number. If the integrated oscillator strength over a range of 0.2eV compressed into line widths of a few meV, then applicability for non-linear optical devices and applications become a reality [9].

Non-linear optical properties are of major interest for photonic device applications such as all optical switching. Intensity dependent changes in the optical properties are prominent at high intensity (I) of pump laser, particularly third order nonlinear effects. Enhanced optical non-linearity has been reported for porous silicon at different wavelengths. Third order nonlinear

effects are generally characterized by non-linear absorption (β) and non-linear refractive index ($n_2$). These are described by:

$$\alpha(I) = \alpha_0 + \beta \mathrm{I} \qquad (1.4.3.1)$$

And $$n(I) = n_0 + n_2(I) \qquad (1.4.3.2)$$

Where, $\alpha_0$ and $n_0$ stands for linear absorption and refractive index, respectively. The β and $n_2$ values are used to evaluate the imaginary ($I_m X^{(3)}$) parts of the third order nonlinear susceptibility. The most versatile technique to measure $I_m X^{(3)}$ and $R_e X^{(3)}$ is the single beam technique, referred as z-scan. The real part of the third-order nonlinear susceptibility is obtained from

$$R_e X^{(3)} = 2n_0^2 \varepsilon_0 C n_2 \qquad (1.4.3.3)$$

Where $\varepsilon_0$ is the permittivity of free space, c is velocity of light and $n_o$ is the effective refractive index. The non-linear absorption arises from either direct multi photon absorption or saturation of single photon absorption. By comparing $R_e X^{(3)}$ and $Im X^{(3)}$ one can conclude that $R_e X^{(3)} >> Im X^{(3)}$ i.e. the non-linearity is mostly refractive. The absolute values of

$$X^{(3)} = \left[ \left( R_E X^{(3)} \right)^2 + \left( I_m X^{(3)} \right)^2 \right]^{\frac{1}{2}} \qquad (1.4.3.4)$$

are significantly larger than the bulk Si values and are of the same orders of magnitude as those reported for p-Si. Due to quantum confinement it is found that the increase in the oscillator strengths caused by the confinement-induced localization of excitons originates the increase of $X^{(3)}$.Figure 1.10 shows the dependence on Si-nc radius r. The scatters could be attributed to effective refractive index and volume fraction of Si-nc in the embedded matrix.

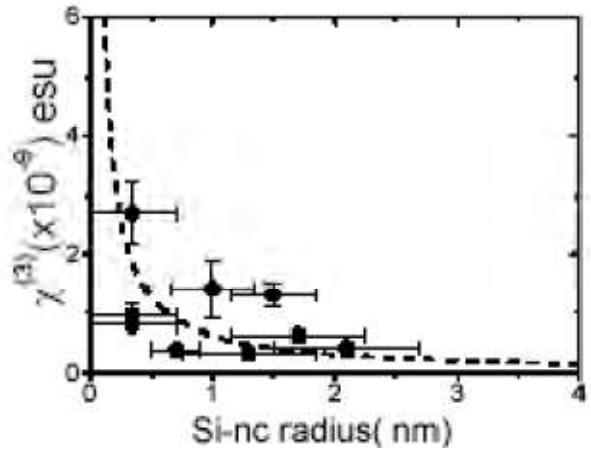


**Figure 1.11:** Variation of χ (3) with Si-nc radius (r) in Si-nc grown by PECVD. Inset shows the PL peak maxima variation with Si-nc radius. Dashed lines are a theoretical [26].

The increase in $X^{(3)}$ follows more closely;

$$X_{Si-nc}^{(3)} = X_{bulk}^{(3)} + \frac{A}{r} + \frac{B}{r} \qquad (1.4.3.5)$$

In reality the experimentally determined $X^{(3)}$ is related to the microscopic by $X_m^{(3)}$

$$X^{(3)} = P \left| f \right|^4 X_m^{(3)} \qquad (1.4.3.6)$$

Where p is the volume fraction and f is a local field correction that depends on the dielectric constant of embedded matrix and nano crystal.

## 1.5 Light Emission from Silicon Nanocrystals and Quantum Confinement Effect

Quantum confinement of electrons and holes within small nanocrystals incorporated into sensitive areas of a device might enhance the photonic capability of Silicon to such a degree that efficient Silicon-based light emitters may be realized. Light can be emitted when an electron recombines with a hole in the semiconductor. To make it efficient, the electron and the hole must be close enough to each other to have overlapping momentum distributions and hence the wavefunction. Unfortunately, this overlap is not possible in a macroscopic Silicon crystal, but when the electron and the hole are confined within the small volume of nanocrystals their positions are defined to such a degree that their momenta become undetermined according to one

of the basic laws of quantum mechanics, the Heisenberg uncertainty relation. Therefore, the momentum distributions of the electron and the hole get smeared-out and overlap, thus enabling light emission.

Quantum confinement effects describe the modification of material properties of precipitates or clusters depending on their size. It is generally known that the band gap increases with decreasing cluster size. This change is large at visible spectral region and hence small changes in cluster size cause large shifts in energy of the emitted photons. If the emission from the device comes from band to band recombination of excitons in the clusters, the band-gap energy determines directly the energy of emitted photon. The enhancement of radiative recombination rate of excitons with decreasing cluster size is another quantum confinement effect. Because silicon is an indirect band-gap material, generated electron-hole pairs have high life- times and they move relatively large distances before recombination. The chance of their combining non-radiatively is high. When the size of the nanoclusters decreases, the number of defects per clusters diminishes. Finally, clusters split to optically active clusters free of defects and optically inactive clusters still containing defects [2].

Reducing the size of a nanocluster also leads to a stronger delocalization of carriers in k-space, and so allows non-phonon assisted transitions [11]. This can be understood when considering Heisenberg uncertainty relations Lifetime of

$$\Delta E \Delta t \geq h \tag{1.5.1}$$

$$\Delta P \Delta x \geq h \tag{1.5.2}$$

the crystal states is in the range of $10^{-10}$- $10^{-9}$ s [3] or more corresponding to the uncertainty in energy E =$10^{-4}$ eV (h = 4.14X$10^{-15}$ eVs). With the band-gap energies of Eg ≈1 eV, the energies of states are well defined. When considering the conservation of momentum equation (1.5) can be rewritten in wavevector form as

$$\Delta K = {}^{2\pi}\!/_{\Delta X} \tag{1.5.3}$$

Separetion of the conduction band energy minimum from the valence band energy maximum is in the range of **2π/a** , where a is a lattice constant (a ≈ 0.5nm). If we add this to the equation (1.5.3) and require that the uncertainty of the momentum Δk must be greater than this, we obtain equation

$$\frac{a}{2\Delta x} \approx 1 \qquad (1.5.4)$$

The uncertainty of momentum increases as the size of the nanocrystal decreases and for d= Δx=0.5 nm the uncertainty of the momentum is as large or larger than 2π/a which is the minimum position of the conduction band in Silicon allowing non-phonon assisted electron transitions. Phonon assisted and non-phonon assisted processes are assumed to be competitive processes and it is also shown that the probability of non-phonon assisted process reaches the phonon assisted at cluster size of 1mm [3]. It can be derived from molecular orbital theory, that when nanocrystal size decreases tight binding of atoms results in discrete states at the boundaries: at the top of the valence bands and bottom of the conduction bands. The separation of these states and the band-gap increases with decreasing crystalline size. It can be thus written that

$$E_g \, \alpha \, \frac{1}{d^{\gamma}} \qquad (1.5.5)$$

where $E_g$ is the energy of the gap and emitted photon, d is the diameter of the crystalline and $\gamma \leq 2$ as we mentioned in section 1.2 and figure 1.4. Quantum confinement is a very attractive emission model due to its simplicity, apparent similarity to the luminescence models from conventional, pn-junction- based LED devices, and because it would introduce an efficient way to control light emission from Silicon-based materials. In reality, the emission model from clusters might be more complicated.

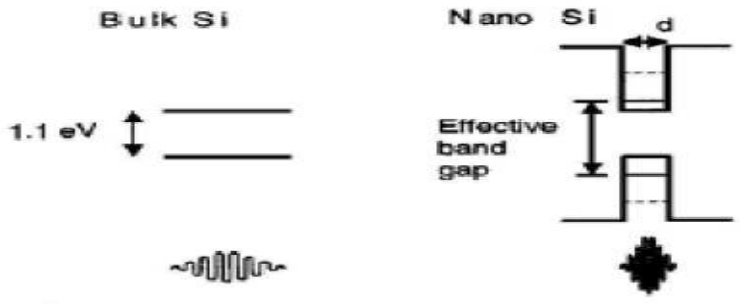


**Figure 1.12:** The increase of the band gap with decreasing crystalline size due to quantum Confinement [62]

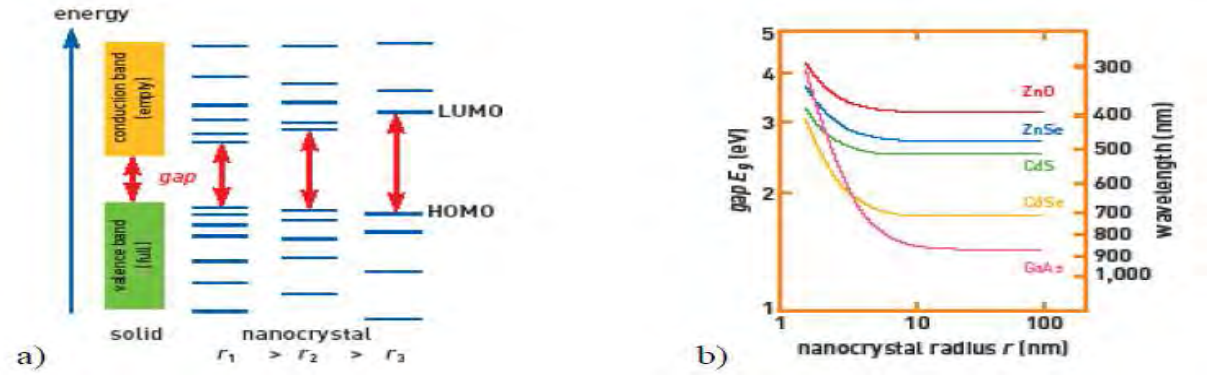


**Figure 1.13:** a) Schematic evolution of the electronic structure between the macroscopic solid and nanocrystal of decreasing size. b) Theoretical variation of the gap calculated from the equation for the nanocrystals of different semiconductors [63].

## 1.6 Quantum Dots, Quantum Wires and Quantum Wells

Progress in epitaxial growth and advances in patterning and other progressing techniques have made it possible to fabricate 'artificial' dedicated materials for microelectronics [10]. In these materials the electronic structure is tailored by changing the local material composition and by confining the electrons in nanometer size foils or grains. Due to the quantization of electron energies, these systems are often called quantum structures. Quantum confinement of excitons may occur in only one direction, in two directions or in all the three directions depending on the shape of the nanostructures. At each confinement direction there corresponds a radical change in the wave function of the particle and as a consequence, a series of discrete levels appear.

**Quantum Dot: -** A quantum dot has all the three dimensions in the nano range. This means, there is a total confinement in each direction and particles cannot move freely anywhere. Thus it is referred to as a 0-D nanostructure.

**Quantum Wire: -** is a 1-D nanostructure where particles are free to move in only one direction. That is two sides of the structure are of nanometer length.

**Quantum Well**: - A quantum well is a nanostructure where there are two directions for the movement of particles, while the third direction determines the quantum confinement direction. It is said to be a 2-D nanostructure.

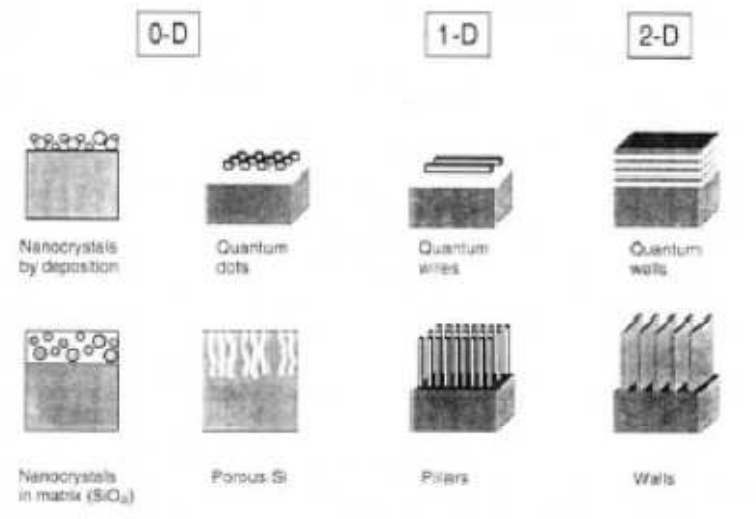


**Figure 1.14:** Schematic of low dimensional Structure [64].

Quantum dots can be obtained by means of different techniques such as chemical vapor deposition (CVD), Ion-implantation, sputter deposition; etc.We will see all these in the next chapter. 1-D structures (quantum wires) can be synthesized by depositing layers of different materials having nanometric dimensions; for example in $Si/Si0_2$ multipliers; $Si0_2$ layers act as a barrier, while excitons are confined in the Si layers. Fig (1.14) gives the nanostructures classification in different dimensions.

## 1.7 Photoluminescence

The optical properties of bulk silicon are mediocre because the light-emission in the bulk is a phonon-assisted indirect process. Therefore, to improve on the light-emission feature in silicon-based materials is a challenge for both technological and fundamental research.

Silicon nanocrystallites (nc-Si) with diameters, d, less than ~5nm exhibit room temperature photoluminescence (PL) due to the recombination of quantum confined excitons which is a result of a significant overlap in electron and hole wavefunctions. Since the strength of the luminescence (i.e, the emission rate and quantum efficiency) depends on the extent of this overlap and the transition probability, a possible means for increasing this overlap for the silicon-based materials may be accomplished through, for example, alloying to change the band

structure, introducing impurities to produce the intermediate state through which the hole, or zone folding to yield the desired quasidirect transition.

According to their surface termination, silicon nanocrystallites can be classified into categories: hydrogen or oxygen terminated. Nanocrystallites of freshly prepared porous silicon belong to the first category, whereas the latter category contains aged and oxidized-surface porous silicon and silicon nanocrystallites embedded in $SiO_2$ thin films. For H-terminated, photoluminescence spectral shows continuous shift of peak energy from the bulk band gap to the visible region with a good agreement with the quantum confinement effect, whereas the photoluminescence spectra of oxidized-surface porous silicon are confined to a specific region.

Generally, silicon nanocrystallites grown by different methods exhibit strong photoluminescence in the red region and progressively shift towards the blue when the mean size decreases. Depending on the size, the photoluminescence of silicon nanocrystals can be tuned from the near infrared (1.38 eV) to the ultraviolet (3.02 eV) i.e as the size of a silicon nanocrystallite structure decreases, the band gap of the material increases due to the quantum confinement effect [Fig.(1.15)].

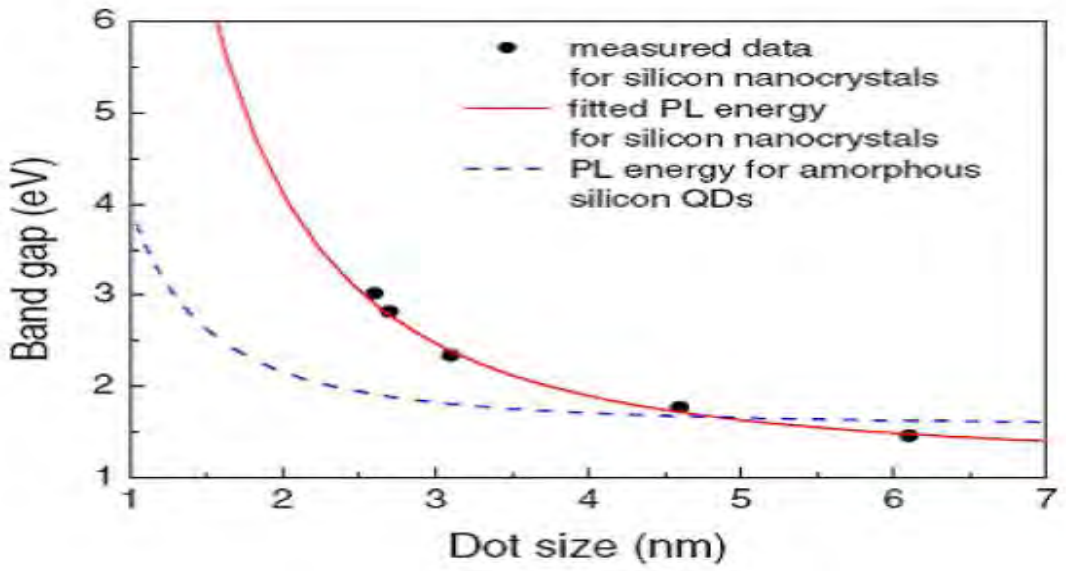

**Figure 1.15:** Photoluminescence peak energy of silicon nanocrystallites as a function of crystal size. The solid line was obtained from the effective mass theory for three dimensionally confined Silicon nanocrystallites[26] .

A blue shift in optical luminescence is the result of quantum confinement effect. Similarly the edge absorption spectra also shift towards the blue with decrease of the silicon nanocrystallites size. However, a quantitative discrepancy between the energy of photoluminescence and the optical band gap calculated from the quantum confinement theory exists.

Figure 1.16 shows a room-temperature photoluminescence spectrum obtained from various sized silicon nanocrystals, where the tuning of the photoluminescence emission from 410 to 900 nm is possible by controlling the size of the silicon nanocrystallite and, as a result, the emission color can be changed by controlling the size of the nanocrystallite. For example, nanocrystallite sizes corresponding to red, green, and blue emission are 4.6, 3.1, 2.7 nm, respectively.

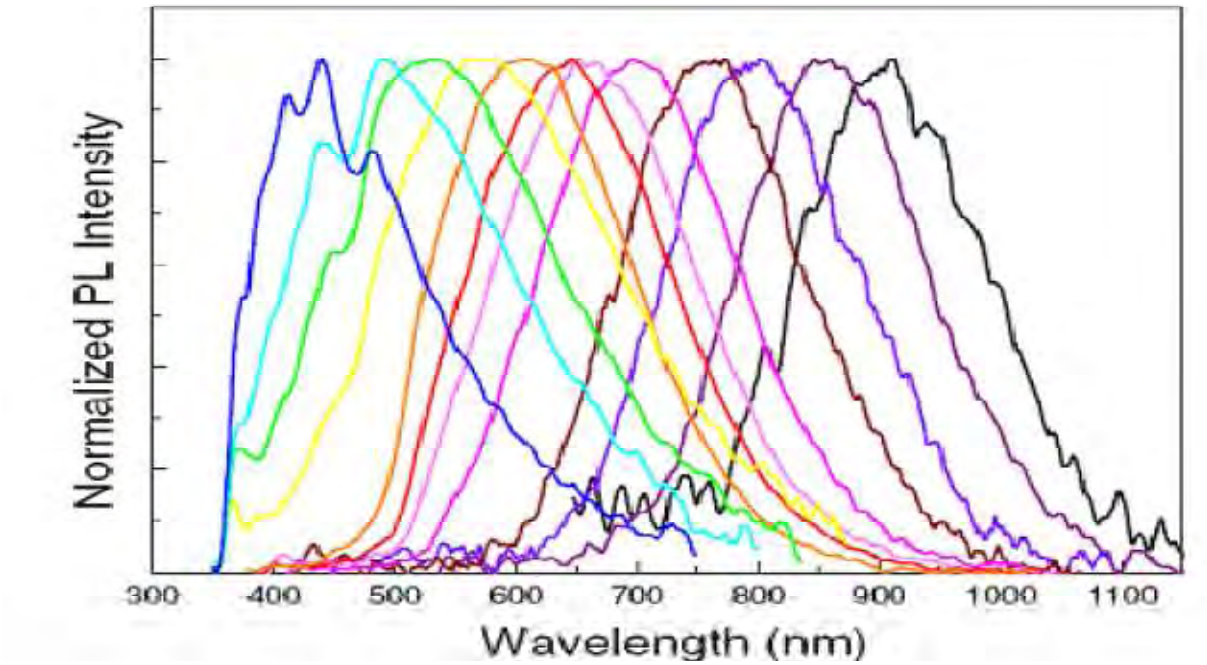


**Figure 1.16:** Room-temperature photoluminescence spectra of silicon nanocrystallites. The peak position can be controlled by appropriate adjustment of the nanocrystallitesize[26] .

## 1.8 Density of states

In order to characterize the physical properties like optical transitions, charge transport etc., the information about the density of states is very crucial [30]. The density of states depends on the dimensionality of the system and the energy versus the corresponding wave vector dispersion relation for the system at hand [31].A general expression for the density of states valid for all types of materials is as a sum delta functions

$$g(E)=\sum_i \delta(E - E_i) \quad (1.8.1)$$

Or

$$g(W)=\sum_k \delta(W - W_k) \quad (1.8.2)$$

For parabolic approximation of the energy versus the corresponding wave vector dispersion relation for the electron or hole we can take a simpler form. Therefore, for a three-dimensional bulk material, the DOS is defined as the number of available electronic states per unit volume per unit energy at energy E and is given by

$$g(E) = \frac{\sqrt{2}}{\pi^2}\left(\frac{1}{\hbar^2}\right) m_e^{3/2} E^{1/2} \quad (1.8.3)$$

Passing from three-dimensional bulk to two-dimensional structures, (so called quantum well) the carrier movement is restricted to a plane. Such two-dimensional systems include thin films, layer structures and superlattices. Now the DOS is modified to the number of available electronic states per unit area per unit energy and is given b

$$g(E) = \frac{m_e}{\pi^2}\left(\frac{1}{\hbar^2}\right) \quad (1.8.4)$$

Further reduction in the dimensionality of the system ends up in a quantum wire. Examples of such one-dimensional structures include nanotubes, semiconductor nanowires, and nanorods. For a quantum wire the DOS is defined as the availability of electronic states per unit length per unit energy and is given by

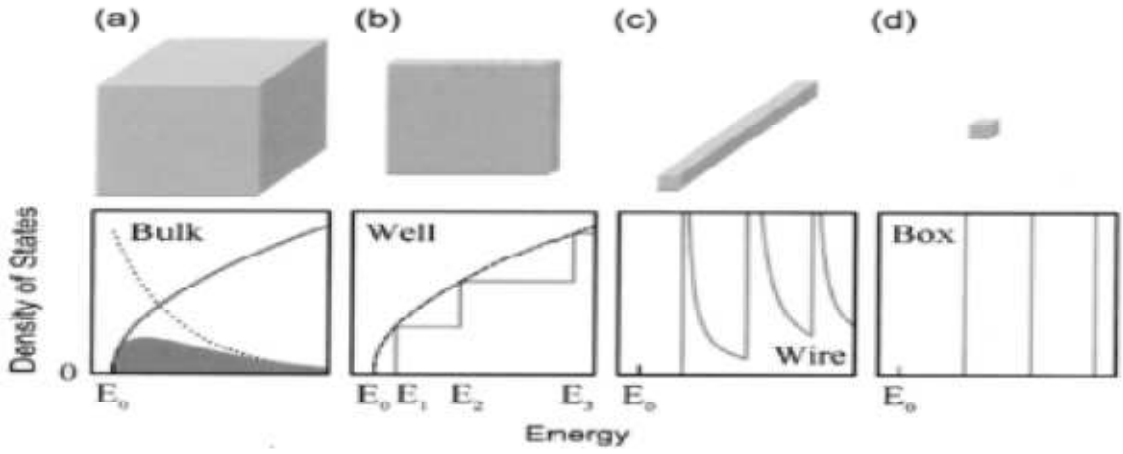


**Figure 1.17:** Density of states for various geometries of semiconductor materials: (a) 3-D bulk, (b) quantum well, a 2-D structure, (c) quantum wire, a 1-D structure, and (d) quantum dot, a 0-D entity. The dotted line in (a) is the thermal distribution of carriers [63].

$$g(E) = \frac{\sqrt{2}}{\pi\hbar} m_e^{1/2} E^{-1/2} \qquad (1.8.5)$$

Finally, for a zero dimensional system (QD), the confinement is along all three dimensions and the DOS becomes a delta function. Figure (1.17) schematically shows the modifications in the DOS as a function of dimension. Transformation from a 3-D bulk system to a 2-D thin film changes the DOS from a continuous parabolic dependence to a step like dependence. This is due to the quantization of carrier motion in the thickness direction. Consequently the optical absorption edge is shifted to higher energy with respect to the bulk and above the absorption edge; the spectrum is stepped rather than smooth [32].In the next chapter we will see how to fabricate synthsis and characterization of silicon nanocristallites.

# Chapter 2

# Fabrication synthesis and characterization of Silicon nanocristals

In this chapter we are going to see Fabrication of silicon nanocrystallites, Preparation of porous silicon, Ion-implanted silicon nanocrystallites, Plasma Enhanced Chemical Vapor Deposition (PECVD) and Characterization of Silicon Nanocrystals to invent silicon nanocristal

## 2.1 Fabrication of silicon nanocrystals

Silicon nanostructures are produced in different ways. Silicon nanocrystallites are generally fabricated by the precipitation of excess silicon in silicon-rich oxides (SRO) which are produced either during deposition, using techniques such as plasma-enhanced chemical vapour deposition (PECVD), or subsequent to the growth of a stoichiometric $SiO_2$ layer by ion-implantation of silicon [21]. Typically, silicon nanocrystallites are obtained by the post annealing of a silicon-rich silicon oxide at $1100^0$C.

Silicon nanocristals embedded in $SiO_2$ can obtained by using several preparetion techniques such as: laser ablation,aerosal teqnique,sputter decomposition,chemical vapour decompsition(CVD) or plasma enhanced chemical decomposition(PECVD).These techniques can be divided into three main approaches: direct synthesis of silicon clusters, formation of a silicon reach layer and subsequent thermal induced phase separation and electrochemical erosion of bulk silicon [26]. Figure 2.1 gives schematics of these techniques

- Laser ablation: - in this method the silicon surface is evaporated by an energetic laser flux and Si-nc are formed by condensation in a gas cell, whose pressure controls, along with the power of the laser pulse the dimensions of Si-nc.
- Aerosol technique: - Here Si-nc are formed and dispersed in a carrier gas flow where they may undergo oxidation processes or also size selection by precipitation.

• Sputtering decomposition: - $Ar^{+}$ ions are used to hit a target made of Si and $SiO_2$. The silicon and oxygen atoms so obtained are then deposited on a substrate in order to obtain SiOx films, from where Si-nc are obtained by a subsequent thermal annealing.

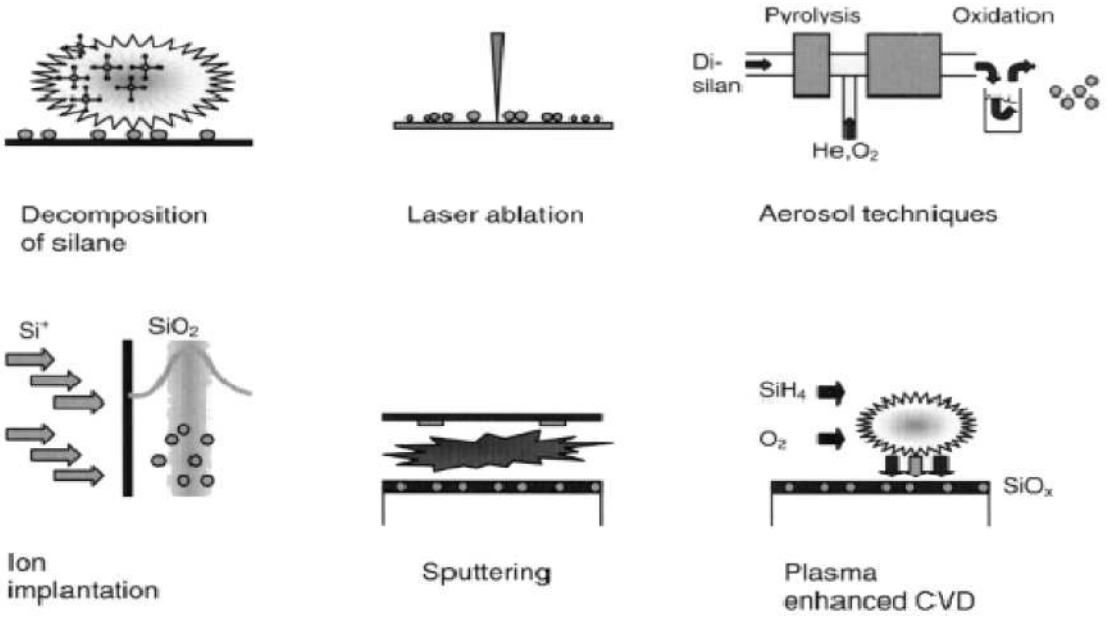


**Figure 2.1:** silicon nanocrystal fabrication techniques [64].

## 2.1.1 Preparation of porous silicon

Porous silicon (PS), whose structural investigations have confirmed that it consists of silicon nanocrystal assemblies of different size (typically a few nm) and shape, is formed by electrochemical anodization of bulk silicon in an HF electrolyte [Figure(2.1)]. The solution employed is typically aqueous 50 percent HF mixed with ethanol. The electrical source chosen for the process is usually current controlled, because the current density and the porosity are directly related. The anodization reaction at the Si/electrolyte interface requires the presence of holes [24]. Therefore, the natural choice for substrate doping is P-type. However, n-type substrates can also be employed for porous silicon fabrication, provided that generation mechanism for excess holes is available. For example, by using light beam, or by biasing the substrate in the breakdown regime.

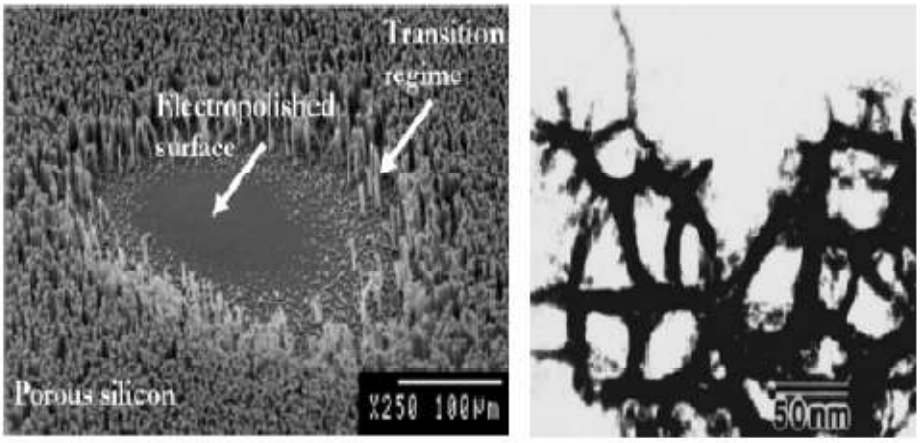


**Figure 2.2:** Formation of porous silicon. (Left) SEM image illustrating the three typical etching regimes in silicon: porous formation, transition regime with pillar-like structures, and electropolishing [25]. (Right) TEM micrograph of porous silicon grains with characteristic size of several nanometers [40].

Depending on the type of doping (p- or n-types) and the doping level of the wafer the sizes of pores and remaining silicon crystallites can be varied from micrometers to nanometers. Porous silicon fabricated on lightly p-type-doped substrates has an average nanocrystal size of 2-5 nm. Since the exciton Bohr radius of silicon is around 4.3nm, quantum confinement effects and in particular, large values of photoluminescence (PL) efficiency are especially evident in this type of porous silicon. On the other hand, in highly p-type-doped wafer (i.e with typical resistivity values around 0.01 cm), the size of the pores and structures is of the order of 10 nm. The quantum confinement effects are in this case less important, thus explaining why the Photoluminescence emission is remarkably weaker in low-resistivity porous silicon. However, carrier transport can be turned over a much wider range, and larger porosity ranges can be obtained. This preparation procedure has attracted much interest due to its simplicity, different from costly litho-graphic or epitaxial techniques that were at the time the conventional approaches to realize nanosized semiconductor [24].

### 2.1.2 Ion-implanted silicon nanocrystals

As the internal surface of porous silicon is enormous, it is also very reactive. This makes porous silicon very interesting for sensor applications but it is a problem when porous silicon is used in photonic devices. Thus alternative techniques have been developed to produce silicon

nanocrystallite (Si-nc). Ion-implanted silicon nanocrystallite can be obtained by implanting silicon into silicon wafers or $SiO_2$ substrates (quartz or thermally grown oxide) and by annealing the samples [Fig.(2.3)].

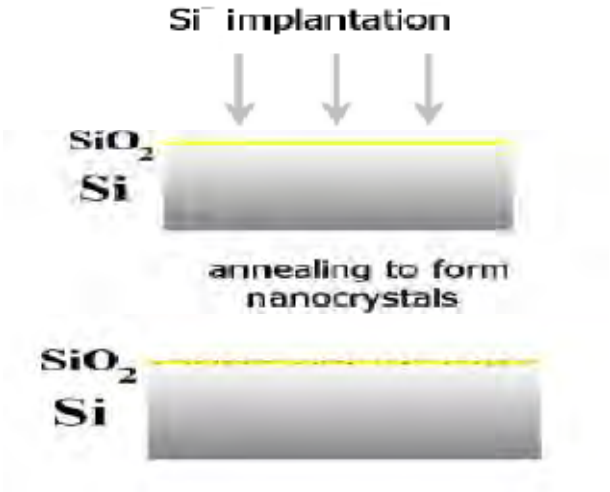


**Figure 2.3:** Formation of silicon nanocrystallites in a $SiO_2$ shell by implantation of silicon ions of 270keV energy into silicon dioxide with subsequent annealing [25].

In contrast to porous silicon, implanted silicon nanocrystallites are very stable and form a reproducible system fully compatible with VLSI technology. The presence of a high-quality $SiO_2$ matrix guarantees superior oxygen passivation of silicon-related dangling bonds and non-radiative centers. In addition, the interface between the silicon nanocrystallite surface and the $SiO_2$ matrix can play an active and crucial role in the radiative recombination mechanism. The silicon nanocrystallite region has an effective refractive index, $n_{eff}$ = 1.71, larger than that of $SiO_2$ [24]. Figure [figure.(2.3)] below shows the formation of silicon nanocrystallites in a $SiO_2$ shell by implantation of silicon ions into $SiO_2$ with subsequent annealing.

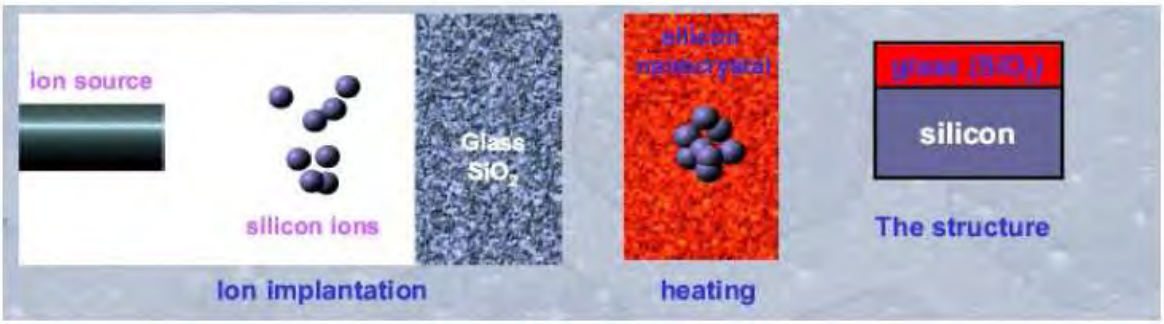


**Figure 2.4:** Synthesis of Si by ion implantation method [67].

### 2.1.3 Plasma Enhanced Chemical Vapor Deposition (PECVD)-grown silicon nanocrystals

This technique is fully compatible with the Si VLSI technology and recently it has been shown that PECVD of sub-stoichiometric silicon oxide ($SiO_x$) layers followed by high temperature annealing represents a quite powerful method to produce Si-nc embedded with in $SiO_{2.}$ PECVD allows the deposition of thin films by using an electric discharge to induce chemical reactions in a gas. The plasma is generated by the application of an rf field to a low pressure gas, thereby creating free electrons within the discharge region. The reactive species generated by the plasma are then adsorbed on the substrate surface, where they are subjected to ion and electron bombardment, rearrangements, reactions with other adsorbed species, new bond formations, leading to film formation and growth.

The deposition process is dependent on the control and optimization of several deposition parameters including rf power density and frequency. Another important parameter in PECVD is the design of the reactor and the electrode configuration. RF tuning networks of PECVD systems usually employ an inductor, which shunts the powered electrode to establish this condition. Figure 2.4a gives the schematic of the apparatus for Si-nc synthesis. It is a PECVD system, consisting of an ultra high vacuum chamber, a load-lock, and 4-gas lines equipped with mass flow meters. An rf generator is connected through a matching network to the top electrode of the

reactor; the bottom electrode is grounded and acts also as sample holder. In the bottom electrode, there are lamps to heat the substrate.

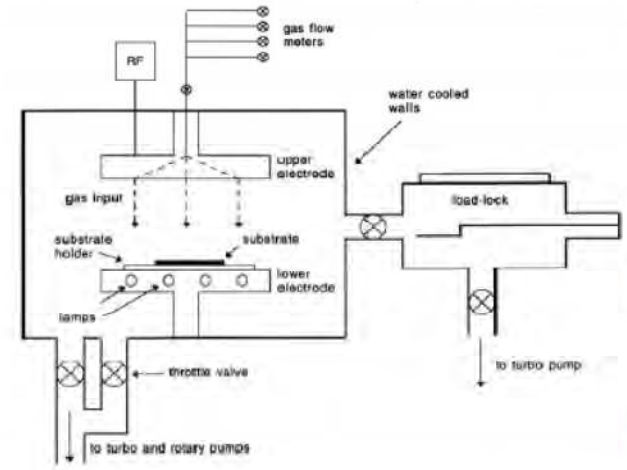


Fig 6.4a

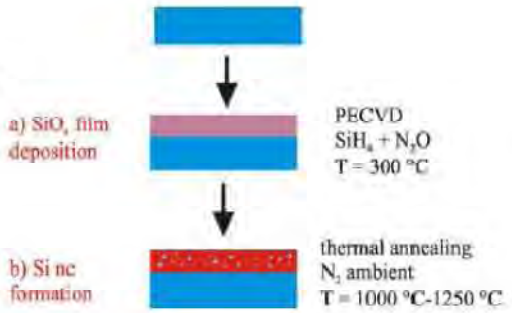


fig 6.4b

**Figure2.5a** scheme of the PECVD aparatus for the Deposition process[68].

**Figure 2.5b)** state of preparetion of Silicon[68].

Figure2.5b) shows the steps for the preparation of Si-nc. The first step is the deposition by PECVD of sub-stoichiometric $SiO_x$ with x<2 on a silicon wafer, by using $SiH_4$ and $N_2O$ gaseous precursors and input power. After deposition, the films were annealed at high temperature to induce the separation of the $SiO_2$ and Si phases from the initial homogeneous SiOx phase and formation of Si-ncs embedded in silicon oxide. The annealing process leads to the formation of Si-ncs, but also to the elimination of the hydrogen because the bonds Si-H are weak and therefore it is possible to break them easily. On the other hand, the Si-N bonds are stable and hence N is not eliminated by the annealing process but it remains embedded in the matrix.

In ion-implantation, plasma or low pressure CVD and sputtering techniques, Si-nc is formed by phase separation [4]. The difference among them is related to the degree of purity of the film (better for ion implanted samples), to the degree of defect incorporated to the porosity of the deposited films (greater for sputtered samples), to the control of the Si-nc content profile (better for the CVD films).

After deposition, the films are thermally treated at high temperature to induce the phase separation between silicon and the dielectrics. If $SiO_2$ is used as a dielectric, typical temperaturesfor the formation of Si-nc are between 900-1200 $^{o}$c.

## 2.2 **Characterization of Silicon Nanocrystals**

Once a sample is synthesized characterization of the size and morphology of the synthesized material is analyzed using AFM, diffraction methods, Raman spectroscopy and surface reactivity method. Silicon nanoparticles formed as deposits or composite materials typically show nearly spherical geometrically in high-resolution transmission electron spectroscopy.

In the synthesis of silicon nano crystals by thermal vaporization of silicon in argon buffer gas followed by exposure to atomic hydrogen to passivate the surface on highly oriented graphite (HOPG) substrate. X-ray diffraction and high-resolution transmission electron microscopy (HRTEM) on these samples verify that nc-Si is indeed crystalline and approximately spherical (Figure2.6a) [15]. The distribution in the diameter of the Si-nc is determined from the z-scale of the AFM image (figure 2.6b)

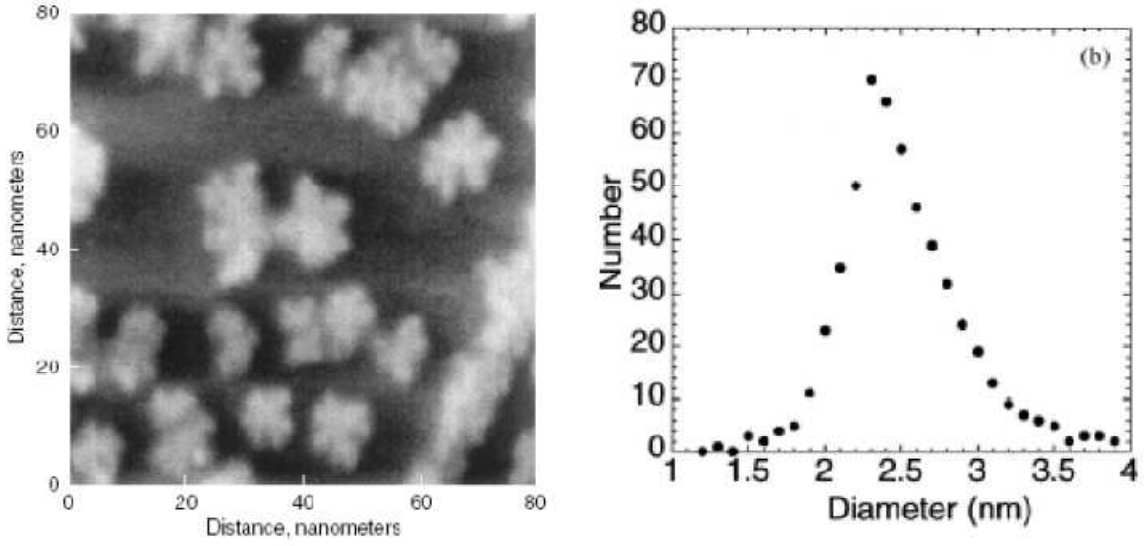


Figure 2.6 :( a) AFM image of Si-nc on the basal plane of HOPG formed by evaporation of at 17000 in argon buffer gas. (b) The size distribution of the Si-nc determined from the AFM height mode [69].

Si-nc fabrications by the precipitation of excess Si in silicon rich oxides (produced by PECVD) produce nanocrystals with mean diameters in the range of 3-5nm.The resulting HRTEM micrograph of Si-nc in $SiO_2$ and the corresponding size distributions are shown in Figure 2.6a and b.

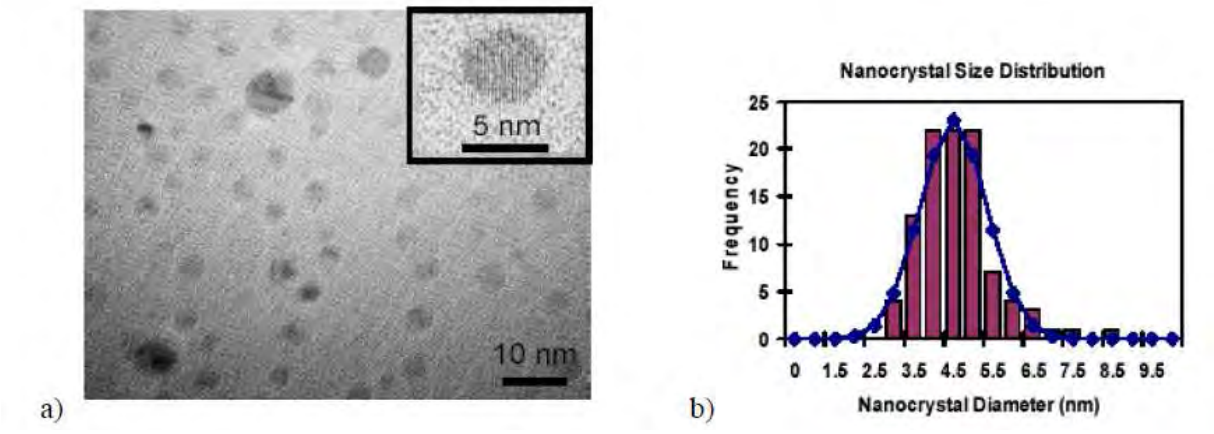


**Figure 2.7 a)** HRTEM micrograph of Si-nc in $SiO_2$.Implant condition; 100KeV Si-; corresponding to an excess Si conc. of 10at. % at projected range of150nm Annealed 1100c; 16hr **b)** Size distribution of Si-nc[70].

In a macroscopic crystal of silicon, one has about $10^{23}$ electrons and nuclei. In principle the application of the known laws of quantum mechanics allows one to predict all the physical and chemical properties of such a system. However, given the astronomical number of particles, it is absolutely hopeless to extract physically meaningful results without some dramatic approximations. The pseudo-potential–DFT is one of these approximation methods the application of which is treated in the next chapter. In adition to that we will see the modeling of silicon nanocristals embedded in a $SiO_2$ matrix and a model of silicon quantem dot.

# Chapter 3

# Theory modeling and simulation of silicon nanosystems

In this unit we will going to see the Pseudo-Potential-density functional theory applied to nanostructures, constructing pseudo-potentials, structures of silicon nanocrystals in a computational approach, modeling of Silicon nanocrystals embedded in a $SiO_2$ matrix and modeling of quantum dot to identify the theorotical aspect.

## 3.1 The Pseudo-Potential-Density Functional Theory Applied to Nanostructures

The pseudo-potential model of a solid has led the way in providing a workable model and modern computers have provided the computational resource to allow the implementation of this method. For example, it is now possible to predict accurately the properties of complex systems such as quantum dots or semiconductor liquids with hundreds, if not thousands of atoms. These first principles pseudo-potentials often relay on density functional theories, which are exact in principle but in practice relay on various approximations such as the local density approximation [5]. The purpose of this chapter is to preview how to implement this approximation method in nanostructures such as that of silicon.

A solution to the electronic structure is obtained in this approach from the Kohn-Sham equation. The Kohn-Sham problem, cast within the pseudo-potential–density functional formalism is easy to solve for simple elemental crystals such as silicon [6].The pseudo-potential model treats matter as a sea of valence electrons moving in a background of ion cores (fig.3.1). The cores are composed of nuclei and inert inner electrons. The ion cores composed of the nuclei and tightly bound core electrons are treated as chemically inert. The pseudo-potential model describes only the outer, chemically active, valence electrons.

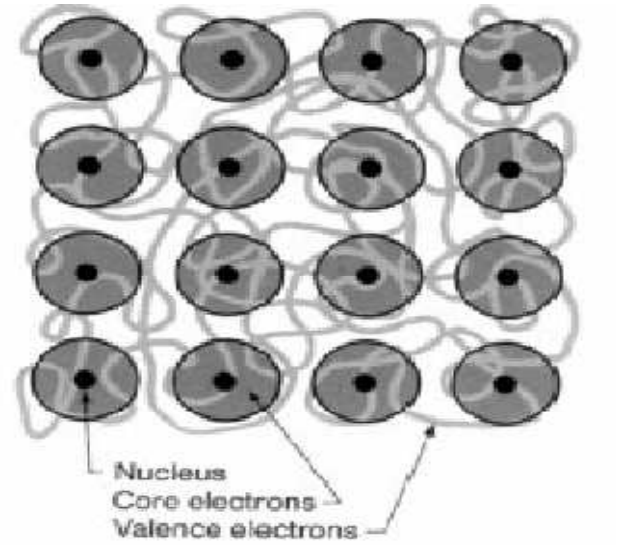


Figure 3.1 Standard pseudo-potential of a solid [71].

### 3.1.1 Constructing Pseudo-potentials

Most pseudo-potential is almost always based on density functional theory (DFT). Within DFT, the many body problems is mapped on to a one-electron Hamiltonian. The effect of the exchange and correlation interactions is subsumed into a one electron potential that depends on the charge density.

This mapping of the many body problems to a one-body problem often incorporates an additional approximation- the local density approximation (LDA). LDA allows one to construct self-consistent field pseudo-potentials for condensed matter systems. The chief limitation of these approximations is that they are appropriate only for the ground state structure and cannot be used to describe excited states without other approximations. As such one uses LDA to determine structural energies, compressibility elastic constants, vibration modes and so on, but not band gap from the eigenvalue spectra [6]. With respect to band gap and electronic excitations, it is possible to consider these by implementing linear response theory on top of standard LDA calculation.

According to the Kohn and Sham approach, for an isolated atom, one can write down a one-electron Hamiltonian and the corresponding one-electron Schrödinger equation using LDA:

$$\{-\hbar^2 \frac{\nabla^2}{2m} - \frac{Ze2}{r} + V_H(r) + V_{xc}[r,\rho(r)]\}\Psi_n(r) = E_n\Psi_n(r) \quad (3.1.1)$$

Where there are Z-electrons in an atom, $V_H$ is the Hartree potential, and Vxc is exchange correlation potentials; $V_H$ and Vxc can be determined from the electronic charge density [7]. The eigenvalue and the eigenfunctions; $E_n$ and $\psi_n(r)$ respectively can be used to determine the total electronic energy of the atoms.

The density is given by:

$$\rho(r) = -e \sum_{n,occup} |\psi n(r)|^2 \quad (3.1.2)$$

$V_H$ is then determined by: $$\nabla^2 V_H(r) = -4e\pi\rho(r) \quad (3.1.3)$$

This term can be interpreted as the electrostatic interaction of the electron with the charge density of the system.

With the DFT, one can define Vxc as a function of the charge density. The central tenant of the LDA is that the total exchange correlation energy may be written as:

$$E_{xc}[\rho] = \int \rho(r) E_{xc}\rho(r) d^3(r) \quad (3.1.4)$$

Where $E_{xc}$ is the exchange correlation energy density; with knowledge of $E_{xc}$, one can extract the potential and the total electronic energy of the system.

It is a common practice to separate exchange and correlation contributions. i.e.,

$$E_{xc} = E_x + E_c. \quad (3.1.5)$$

It is also convenient to define an electron gas parameter, $r_s$ where $r_s$ is given by;

$$r_s = \left(\frac{3}{4\pi\rho(r)}\right)^{1/3} \quad (3.1.6)$$

A simple form of Ex can be obtained by evaluating the potential for a homogeneous electron gas:

$$E_x(r_s) = \frac{0.4582}{r_s} \quad (3.1.7)$$

For the correction contribution ($E_c$) to this potential, different forms have been proposed. One of the most popular arises from Monte Carlo simulation on free electron- gas. The results from the simulation are numerically parameterized for convenient implementation.

One commonly used form is:

$$E_c(r_s) = -\frac{0.1432}{1+1.0529\sqrt{r_s}+0.334rs} \qquad \text{for } r_s \geq 1 \quad (3.1.8)$$

And $E_c(r_s) = -0.o480+0.0311 \ln r_s-0.0116r_s+ 0.0020r_s \ln r_s$ for $r_s <1$ (3.1.9)

Once $E_{xc}$ is known, the potential energy can be obtained from the functional derivatives:

$$V_{xc}[r, \rho(r)] = \frac{\partial E_{xc}}{\partial r_s}(r_s).\frac{\partial r_s}{\partial p} \quad (3.1.10)$$

This potential can be explicitly written as;

$$V_{xc}[r, r_s] = E_{xc}[r, r_s] - \frac{r_s}{3}(\frac{dE_{xc}}{dr_s}) \quad (3.1.11)$$

It is not difficult to solve Eq. (3.1.1), the Kohn-Sham equation, for an atom. The charge density is taken to be spherically symmetric. Thus, the problem reduces to solving a one-dimensional problem. $V_H$ and $V_{xc}$ can be iterated to form a self-consistent field. Kerker proposed a straightforward method for constructing a local density pseudo-potential that retained the norm-conserving criterion. He suggested that the pseudo wavefunction has the form:

$$\varphi_p(r) = r^l \exp p(r) \qquad \text{for } r< r_c \quad (3.1.12)$$

Where $P(r)=-ar^4-a_1r^3-a_2r^2-a_3$ is a polynomial and

$$\varphi_p(r) = \Psi_{AE}(r) \qquad \text{for } r<r_c \quad (3.1.13)$$

While all local density pseudo-potentials impose the condition that

$$\varphi_p(r) = \Psi_{AE}(r) \qquad \text{for } r<r_c$$

the construction for $r < r_c$ is not unique.

One straightforward approach to optimize pseudo-potential is to build additional constraints into the polynomial given in Eq.3.1.12. For example, suppose we write

$$\rho(r) = C_o + \sum_{n=1}^{N} c_n r^n \qquad \text{(in Kerker's scheme N=4)} \quad (3.1.14)$$

Once the pseudo-wave function is defined as in Eqs. (3.1.12) and (3.1.13), we can invert the Kohn-Sham equation and solve for the ion core pseudo-potential, $V_{ion}$, p.

Since the ion cores can be treated as chemically inert and highly localized, it can be written as:

$$V_{ion}(r) = \sum_{R_a} V_{ion,a}(r - R_a) \quad (3.1.15)$$

Where $V_{ion}$ is the ion pseudo-potential associated with the atom, a, at a position $R_a$.

This potential, when self consistently screened by the pseudo charge density;

$$\rho(r) = -e\sum\left|\varphi_{p,n(r)}\right| \tag{3.1.16}$$

will yield an eigenvalue of $E_n$ and a pseudo-wave function $\varphi_{p,n}$. The pseudo-wavefunction by construction will agree with all the electron's wave functions away from the core. With the eigenvalue problem solved, the total energy of the system, $E_{tot}$, can be evaluated from;

$$E_{tot}= \sum E_n - \frac{1}{2}\int d^3r\rho(r)V_H[r, \rho(r)] + \int d^3r\rho(r)E_{xc}[r, \rho(r)] - V_{xc}[r, \rho(r)] + E_{i\text{-}i}[R_a] \tag{3.1.17}$$

Where, $E_{i\text{-}i}$ is the ion–ion repulsion. If one knows the behavior of the total energy as a function of atomic position, it is possible to compute inter atomic forces and perform *ab initio* molecular dynamics. Since the pseudo-potential is weak, simple basis sets such as a plane wave basis can be quite effective for crystalline matter. For example, in the case of crystalline silicon only 50-100 plane waves need to be used. The resulting matrix representation of the Schrödinger operator is dense in Fourier (plane wave) space. The matrix vector product operations are performed with the help of fast Fourier transforms (FFT). The plane wave method uses a basis of the form;

$$\psi_k(r) = \sum_G \alpha(K,G)\exp(i(K+G)) \tag{3.1.18}$$

Where K is the wave vector, G is a reciprocal lattice vector and ($G$, $K$) α represents the coefficients of the basis.

An alternative approach is to avoid the use of a basis .For instance; one can use a real space method that avoids the use of a plane wave and FFTs altogether. Here a particular version of this approach called the finite-difference pseudo-potential method is illustrated. This approach utilizes finite difference discretization on a real space grid. If a uniform grid is imposed on a system where the points are described in a finite domain by ($x_i$, $y_j$ ,$z_k$) we approximate $d\psi^2(x)/dx^2$ at ($x_i$, $y_j$, $z_k$) by ;

$$\frac{\partial^2\Psi}{\partial x^2} = \sum C_n\psi(x_i + y_j + z_k) + O(h^{2M+2}) \tag{3.1.19}$$

Where h is the grid spacing and M is a positive integer. This approximation is accurate to o ($h^{2M+2}$) upon the assumption that ψ can be approximated accurately by a power series in h.

With the kinetic energy operator expanded as in Equation (34) one can set up a one electron Schrödinger equation over a grid [5, 6, 7]. The wave function $\psi(x_{i,},y_i)$ is computed on the grid by solving the eigenvalue problem;

$$\frac{-\hbar^2}{2m}\{\sum_{n_1=-M}^{M} C_{n1}\,\Psi_n(x_i+n_1h\,,y_j\,,z_k) + \sum_{n_2=-M}^{M} C_{n2}\,\Psi_n(x_i+y_j,\,n_2h,\,z_k)+\sum_{n_3=-M}^{M} C_{n_3}\,\Psi_n(x_i+y_j\,,z_k\,,n_3h)\}$$
$$+V_{ion}(x_i\,,y_j\,,z_k) + V_h(x_i\,,y_j\,,z_k) + V_{xc}(x_i\,,y_j\,,z_k)\,\Psi_n(x_i\,,y_j\,,z_k) = E_n\Psi_n(x_i,y_j,z_k) \qquad 3.1.20$$

If we have L grid points, the size of the full matrix resulting from the problem is L x L. Each grid point corresponds to a row in the matrix. Fig.3.2 gives a uniform grid illustrating a typical configuration. However many points in the cube are far from any atom in the system and the wave function on these points may be set equal to zero. In the discrete form, the non-local term becomes a sum over all atoms, a, and quantum numbers (l, m) of rank one updates.

$$V_{ion} = \sum_a V_{loc,a}\,a + \sum_{a,l,m} C_{a,l,m}U^T_{a,l,m} \qquad (3.1.21)$$

Where $u_{a,l,m}$ are sparse vectors which are only non-zero in a localized region around each atom, and $C_{a,l,m}$ are normalization coefficients.

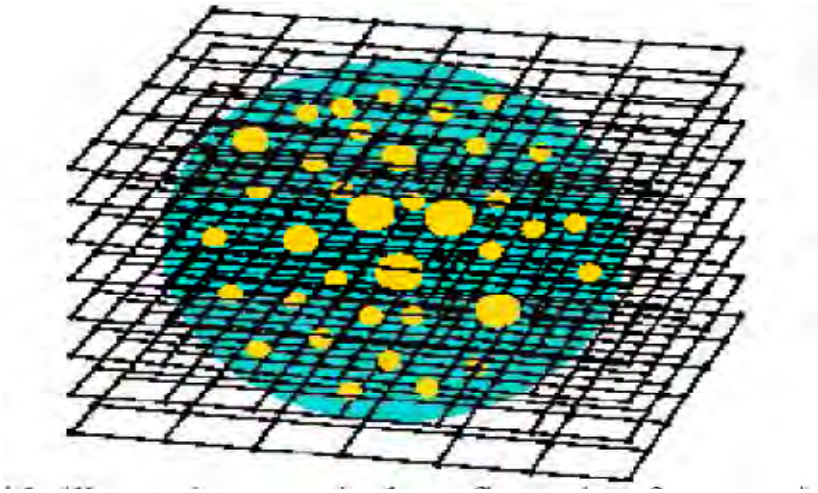

Figure 3.2 Uniform grids illustrating a typical configuration for examining the electron structure of a localized system. The gray sphere represents the domain where the wave functions are allowed to be non-zero. The light spheres within the domain are atoms [72].

A popular form of extracting the eigen pairs is based on the generalized Davidson method in which the pre-conditioner is not restricted to be a diagonal matrix. Pre-conditioning technique in this approach are typically based on filtering ideas and the fact that the Laplacian is an elliptic operator. The eigenvectors corresponding to the few lowest eigenvalues of $\nabla$ are smooth functions and so are the corresponding wave functions. When an approximate eigenvector is known at the points of the grid, a smoother eigenvector can be obtained by averaging the value at every point with the values of its neighboring points. Methods based on approximation inverse techniques have been somewhat more successful, performing better than filtering at additional preprocessing and storage cost. However, filtering techniques are inexpensive to apply and result in substantial savings in iterations.

## 3.2 **Structures of Silicon Nanocrystals–A Computational Approach**

Nanocrystals possess properties that are characteristic of neither the atomic nor solid states. For example, the energy levels in atoms may be discrete and well separated in energy relative to KT. In contrast, solids have continuum of states (energy bands). Clusters may reside between these limits, i.e., the energy levels may be discrete, but with a separation much less that KT.

The most fundamental issue in dealing with nanocrystals is determining their structure. Before any accurate theoretical calculations can be performed for a cluster, the atomic geometry of a system must be defined. Real space methods are easily suited for investigating these systems. Serious problems arise from the existence of multiple local minima in the potential energy surface of these systems; many similar structures can exist with vanishing small energy differences. A complicated issue is the transcriptions of inter atomic forces in to tractable classical force fields. This transcription is essentially difficult for clusters such as those involving semi-conducting species. In these clusters, strong many body forces can exist that preclude the use of pair wise forces.

A convenient method to determine the structure of small or moderate sized clusters is simulated annealing. Within this technique, atoms are randomly placed within a large cell and allowed to interact at a high (usually fictive) temperature. Langevein molecular dynamics is well suited for

simulated annealing methods. In Langevein dynamics, the conic positions, Rj, evolve according to;

$$M_j \ddot{\bar{R}}_j = \bar{F}(R_j) - \gamma M_j \dot{\bar{R}}_j + G_j \ldots \tag{3.2.1}$$

Where (**F (R$_j$)** is the inter-atomic force on the j-th particle, and **M$_j$** ) are the ionic masses. The last two terms on the right hand side of Eq. (3.2.1) are the dissipation and fluctuation forces, respectively [7]. The dissipative forces are defined by the friction coefficient γ. The fluctuation forces are defined by random Gaussian variables, ***G$_j$*** with a white noise spectrum:

$$< G_i^{\alpha}(t)> = 0 \text{ and } < G_i^{\alpha}(t)> <G_j^{\alpha}(t')> = 2\gamma M_j k_B T \delta(t - t') \tag{3.2.2}$$

The angular brackets denote ensemble or time averages, and α stands for the Cartesian component. The coefficient of T on the right hand side of Eq.3.2.2 insures that the fluctuation-dissipation theorem is obeyed, i.e., the work done on the system is dissipated by the viscous medium.The inter atomic force $F_i^{\alpha}$ , on an atom located at **R$_a$** in the α direction for a finite system is obtained using the Hellmann Feynman theorem;

$$F_a^{\alpha} = - \frac{dE_{tot}}{dR_a^{\alpha}} = - \frac{\partial E_{e-i}}{\partial R_a^{\alpha}} = - \frac{\partial E_{i-i}}{\partial R_a^{\alpha}} \tag{3.2.3}$$

Where $E_{tot}$ is the total ground state energy.

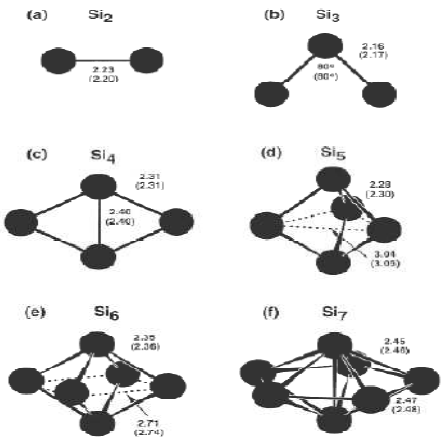


Figure 3.3 Ground state geometries and some low-energy isomers $Si_n$ (n≤7) clusters[34].

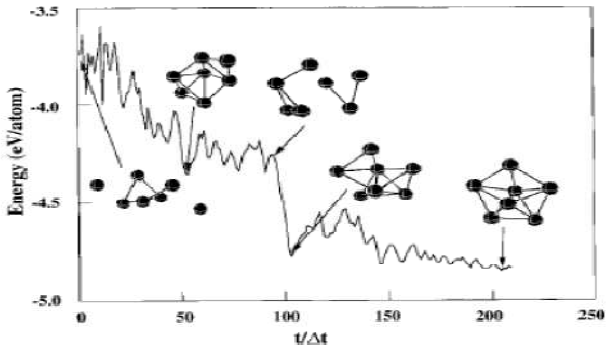


Figure 3.4 Binding energy of $Si_7$ during a Langevein Simulation[73].

The inter-ionic core interaction is simply the point-charge interaction. Once the inter atomic forces are determined, it is straight for word to implement simulated annealing. An initial atomic configuration is chosen and the system is then heated to a high temperature. As the system is cooled, only lower energy structures form. If the anneal is done slowly, it is possible to achieve the ground state structure. Figure 3.4 gives the ground state structure of silicon cluster of seven atoms, which is obtained by simulated annealing procedure. Figure 3.3 presents the ground state structures for sin for$7 \leq n$.

## 3.3 modeling of Silicon nanocrystals embedded in a $SiO_2$ matrix

In this section our goal is to build up a simple model to study the properties of Si nanocrystals embedded in $SiO_2$ matrix from a theoretical point of view. [55] In Fig. 3.5 the HOMO and LUMO isosurfaces at the fixed value of 10% are reported; we clearly see that the distribution is totally confined in the Si-nc region with some weight on the interface O atoms. These features are entirely new, they do not exist for the isolated cluster or for the pure matrix, and so have to be due to the nature of the interface region.

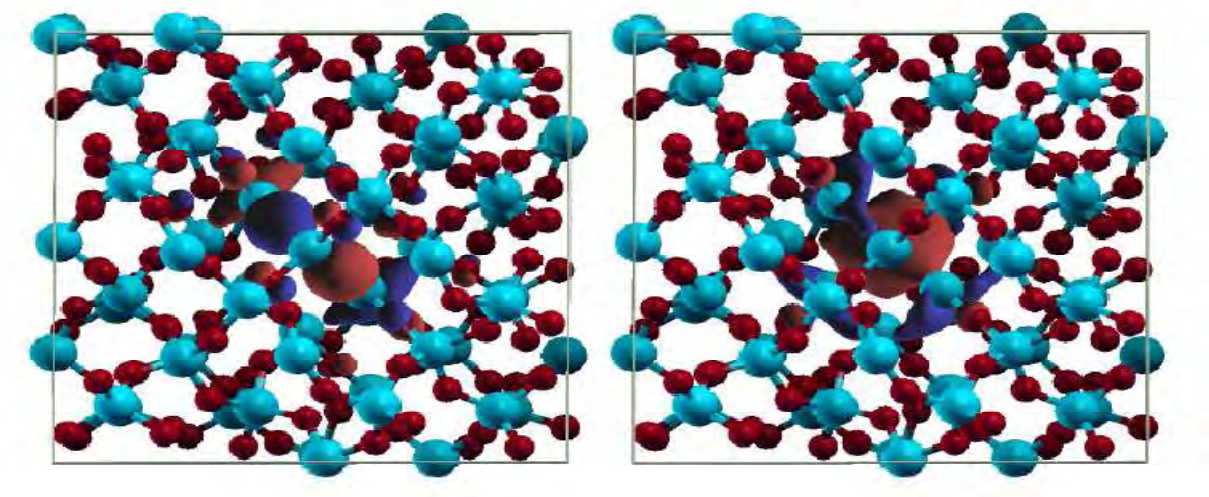

**Fig. 3.5:** The optical gain spectrum for the $Si_{10}$ nanocluster embedded in a $SiO_2$ matrix in the low energy region.

The origin of the PL observed in the red optical region for Si-nc immersed in a $SiO_2$ matrix can then be found in the properties of this interface. Our result concerning the role of both Si-nc and the interface Si-O region with respect to the absorption process is in close agreement with the X-ray absorption fine structure measurements that indicate the presence of an intermediate region between the Si-nc and the $SiO_2$ matrix about 1 nm thick that participates in the light emission process.

## 3.4 Modeling the Quantum Dot.

Silicon dots can be modeled by considering a bulk-terminated cluster of Si atoms caped off by H atoms (or H-like atoms) [8]. The dangling bonds are saturated with hydrogen like atoms. A ball and stick model of a silicon quantum dot is shown in figure 3.10.

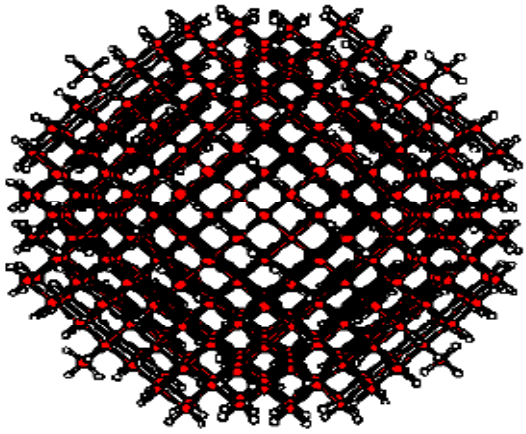

Figure 3.6: Atomic structure of a Si quantum dot with composition $Si_{525}H_{276}$ [74].

In the next chapter we will see silicon nanocristal for photonic application.

# Chapter 4

# Silicon nanocristals enabling silicon photonics

In this chapter we are going to see Silicon photonics of wave guide,modulators,sources,and detector.In addition to these we will see Si-nc waveguides.

## 4.1 Silicon Photonics

Copper interconnects will soon be the limiting factor of the performance of a computer. The aim of Silicon Photonics is to bring the high performance of optical interconnects to silicon, a relatively cheap and abundant resource.

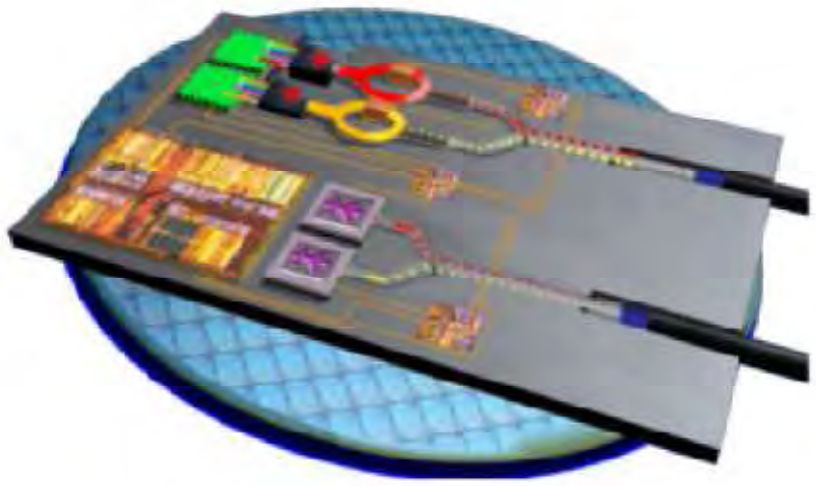

**Figure 4.1:** Intel's vision of an integrated silicon phonics chip[75].

Today optical data connections are most commonly found in long haul communications and in large server farms. These connections make up the backbone of our communications infrastructure because of their ability to transfer massive amounts of data at the fastest rate possible. Due to the high price of a single optical connection the optical interconnect market

typically ends here. This high price is typically due to the exotic materials from which optical devices are constructed.

Current interconnect technology uses electrical signals sent along copper wire to transfer data between high speed fiber optic connections and the users to whom the data is being sent. Copper is also used as the core interconnects technology inside computers. Unfortunately copper is reaching its peak performance and the only way to transfer greater amounts of data using electrical signals is to have more connections. While this is currently not a major problem facing the majority of today's technology this limitation of copper poses a serious threat to future of microprocessor manufacturers.

Silicon Photonics is a relatively new field with the goal of developing silicon based optical devices. This approach appears to be very enticing due to multiple reasons including the large established silicon fabrication infrastructure and the relatively low cost and high abundance of this material. Unfortunately silicon does not have inherently good optical properties, however many of these short comings are proving to be engineering problems and not absolute limitations.For the development of an integrated optical chip consisting of six significant components: waveguides, optical modulator, laser source, photo-detector, CMOS intelligence, and passive assembly.

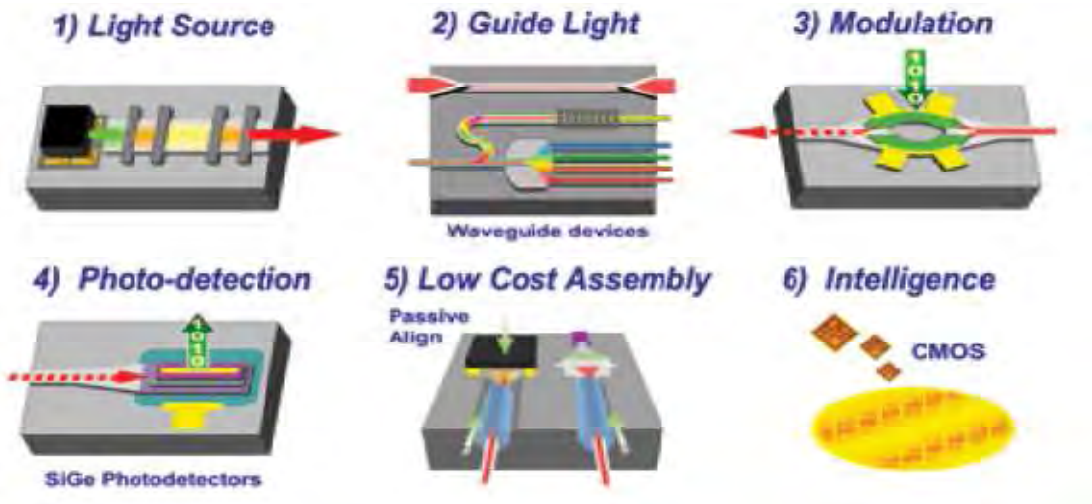


**Fig4.2:**The building blocks of the integrated optical circuit[75].

## 4.2 Silicon Waveguides

Silicon waveguides are the first piece of the silicon photonics vision. The ability of silicon to guide light depends on many key properties of the material. The band gap of silicon determines the shortest possible wavelength of light able to propagate through the material without being absorbed. The band gap of silicon is approximately 1eV which correlates to a wavelength of 1.24μm; below this wavelength silicon becomes opaque. The wavelengths used in silicon photonics lie in the range of 1.3μm to 1.6μm which encompasses the 3 bandwidths commonly used in fiber optic communication systems: the C-band (1.53μm - 1.562μm), the S-band (1.485μm - 1.52μm), and the L-band (1.57μm - 1.61μm).

Waveguides and optical fibers operate based on the concept of total internal reflection (TIR), where light incident on a surface below a certain angle will be entirely reflected back into the waveguide rather than being transmitted in the surrounding medium. TIR is based on the difference between the index of refraction of the waveguide and its surrounding medium, the larger the difference in refractive indices, the smaller the angle required to maintain TIR. A major advantage of silicon is its relatively high refractive index of n=3.45. Silicon dioxide on the other hand, has an index of refraction of n=1.5 and is used as the surrounding medium around a silicon waveguide. The difference between these materials correlates to an index difference of nearly $\Delta n \approx 2$. This property allows for very small devices and tight bends in waveguides.

The basic silicon waveguide is a rib waveguide where a silicon rib is raised above a silicon base resting on an insulating layer; these waveguides are commonly referred to as SOI rib waveguides. Multiple silicon waveguide devices such as Y-splitters, Couplers, Gratings, and Arrayed Waveguides have already been demonstrated.

## 4.3 Silicon Modulator

A digital signal is imposed on light through one of two methods, direct and external modulation. In direct modulation the light source is repeatedly switched on and off, while in external modulation a continuous beam is blocked or forced to interfere deconstuctively. The silicon

modulator is an external modulator based on the design of a Mach-Zender interferometer, where an incoming beam of light is split in half and the two resulting beams travel through two different arms of the interferometer. Along these arms a voltage is applied which induces the Kerr effect, the Franz-Keldysh effect, provides a carrier injection. These three mechanisms provide the same result, a change in the refractive index. By controlling the refractive index the phase of the light can be changed so that when the two arms recombine they either add constructively or deconstructively, thus allowing for modulation of the light.

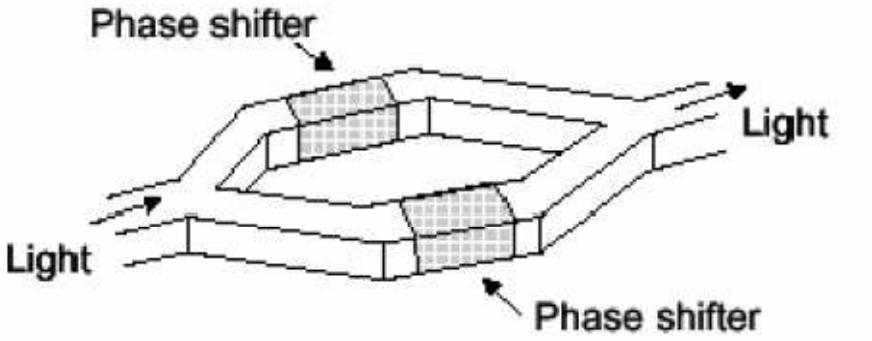


**Fig 4.3:**Schematic of a Mach-Zender interferometer modulator with two phase shifter sections[75].

The Kerr Effect is a second-order electric field effect in which the refractive index is changed proportionally to the square of the applied electric field. The index change is calculated as:

$$\Delta n = \frac{1}{2} S_{33} n_0 E^2 \tag{4.3.1}$$

where $s_{33}$ is the Kerr coefficient and $n_0$ is the unchanged refractive index of the medium.

The Franz-Keldysh effect is due to distortion of the energy bands of the semiconductor upon application of an electric field. Unfortunately the Franz-Keldysh effect falls off greatly for 1.3μm light, and the resulting index shift of the Kerr effect at the application of 100V/μm is only abou - $10^{-4}$. The third method mentioned has a far greater impact on the index of refraction of the material and is given by the equation:

$$\Delta n = \frac{-e^2}{8(\pi c)^2}\left(\frac{\lambda_0^2}{n\varepsilon_0}\right)\left(\frac{N_e}{m_{ce}^*} + \frac{N_h}{m_{ch}^*}\right) \tag{4.3.2}$$

At a wavelength of 1.55μ this simplifies to:

$$\Delta n=\Delta n_e+\Delta n_h=-[8.8X10^{-22}\Delta N_e+6.0X10^{-18}(\Delta N_h)^{0.8}] \quad (4.3.3)$$

At a wavelength of 1.3μm the equation becomes:

$$\Delta n=\Delta n_e+\Delta n_h=-[6.2X10^{-22}\Delta N_e+6.0X10^{-18}(\Delta N_h)^{0.8}] \quad (4.3.4)$$

In the above equations ΔN refers to the number of carriers injected or depleted through this process. Δn refers to the change in refractive index. The resulting phase shift of through these processes can be determined by a much simpler formula corresponding to the effective refractive index, the wavelength, and the length of the phase shifter:

$$\Delta\phi = \frac{2\pi}{\lambda}\ \Delta n_{eff} L \quad (4.3.4)$$

## 4.4 Silicon Laser

The silicon laser is one of the most challenging aspects in this field; this is due to silicon's indirect band gap. The radiative recombination coefficient of silicon is very small (especially when compared to InP, GaAs, or other III-V materials), this implies that stimulated emission in silicon is very unlikely. Through another process known as Raman Effect or Raman Scattering, light can be amplified in silicon however the resulting additional photons generated through the amplification process are quickly absorbed due to long free carrier lifetimes.

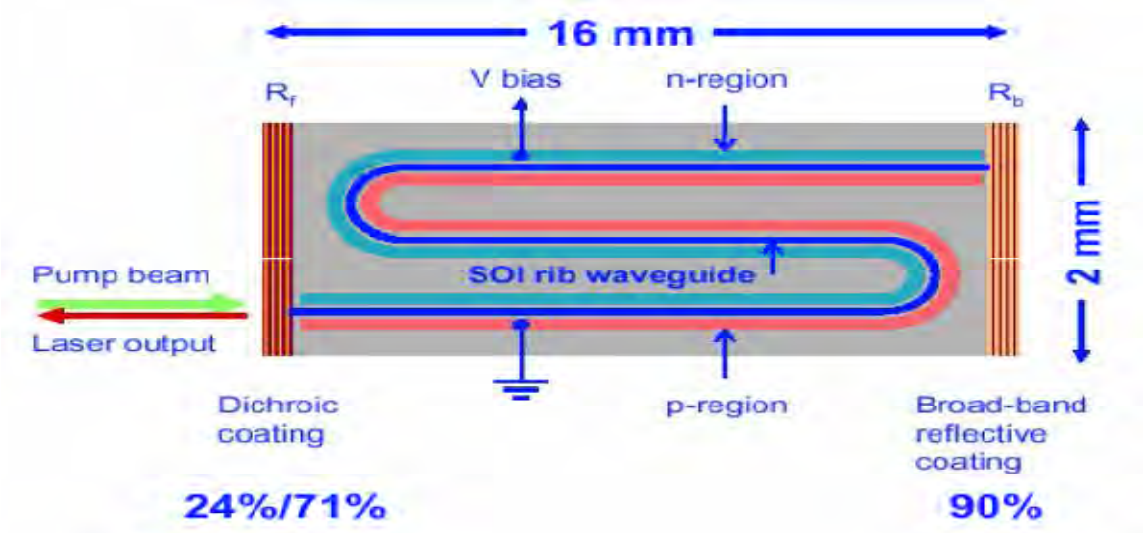


**Fig 4.4:** Top-down schematic of Intel's silicon laser[75].

To reduce the life time of free carriers, a P-I-N structure is created across the waveguide by placing a P-type silicon rail along one side of the waveguide and an N-type silicon rail along the opposite side. When a voltage bias is place across the waveguide, free carriers are swept out of the waveguide and thus amplification can occur.

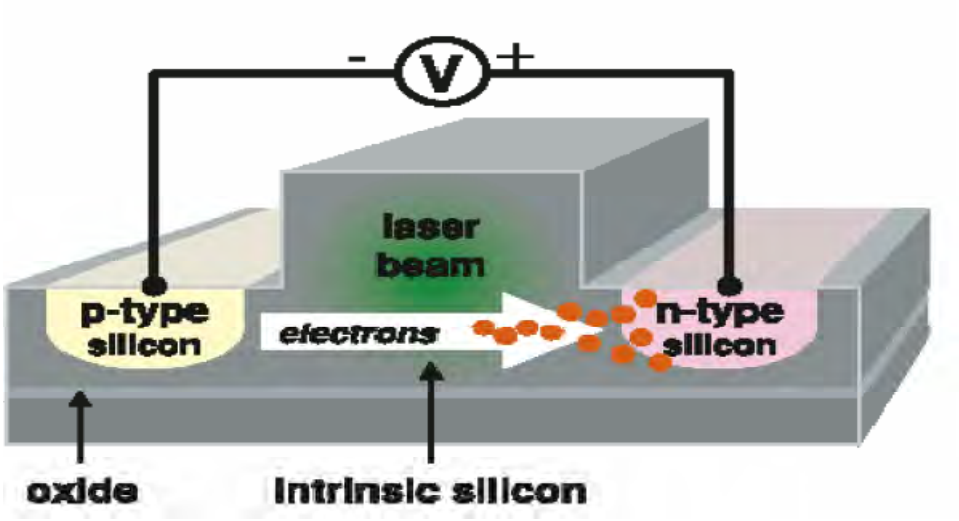


**Fig 4.5:**Silicon Laser used in Intel's experiments[75].

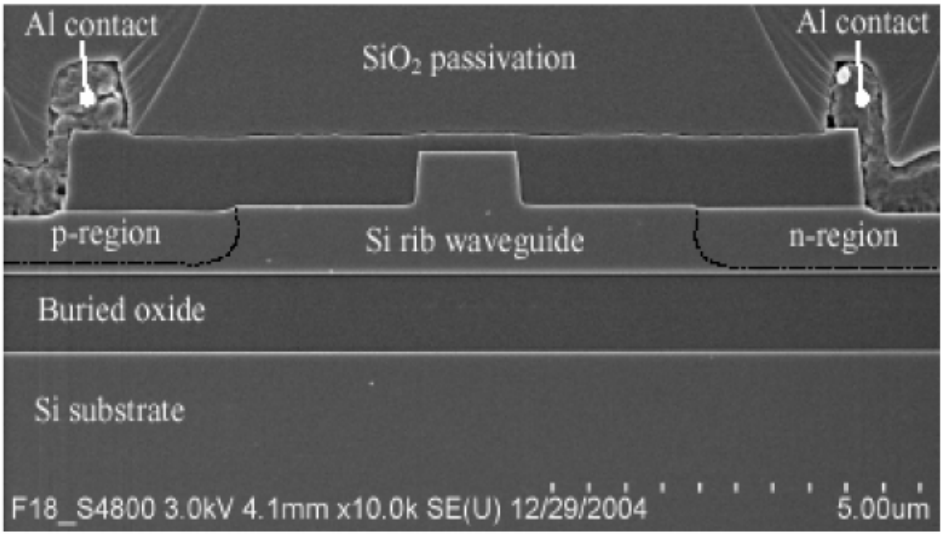


**Fig4.6:**SEM image of Intel's Silicon Laser[75].

Through the Raman Effect, an optically pumped cavity will produce amplification in the light intensity at a wavelength (1.63μm) which is shifted from the wavelength of the pumping source (typically pumped at 1.55μm). The energy of a pump photon is split between a red-shifted photon and a phonon. Raman amplifiers and lasers are common in the telecom industry by using other materials, most commonly glass fiber. A major advantage of using silicon is the Raman gain coefficient, which is 10,000 times greater in silicon than in glass fibers. The amplification gained in a half kilometer of glass fiber can be accomplished in 5 centimeters of silicon. At both ends of the waveguide, mirrors are added to trap this specific wavelength inside the waveguide. The constantly reflected beam builds an optical standing wave inside the resonator cavity. One of the end mirrors is only partially reflective so that when a critical intensity is reached the laser beam can escape the chamber in the form of monochromatic coherent light.

## 4.5 Silicon Photo-Detector

Once light is produced and a signal is impressed in the beam, the data travels to its destination and needs to be converted back into an electrical signal. This is the purpose of a photo-detector. Due to the band gap and for the same reason that silicon is transparent in the optical communication bandwidths, silicon is not a good photo-detection material for infra-red. While Silicon is not a good IR photo-detector germanium is much more responsive in this range. Germanium can be implanted into strained silicon to shift the band gap to make it capable of IR photo-detection.

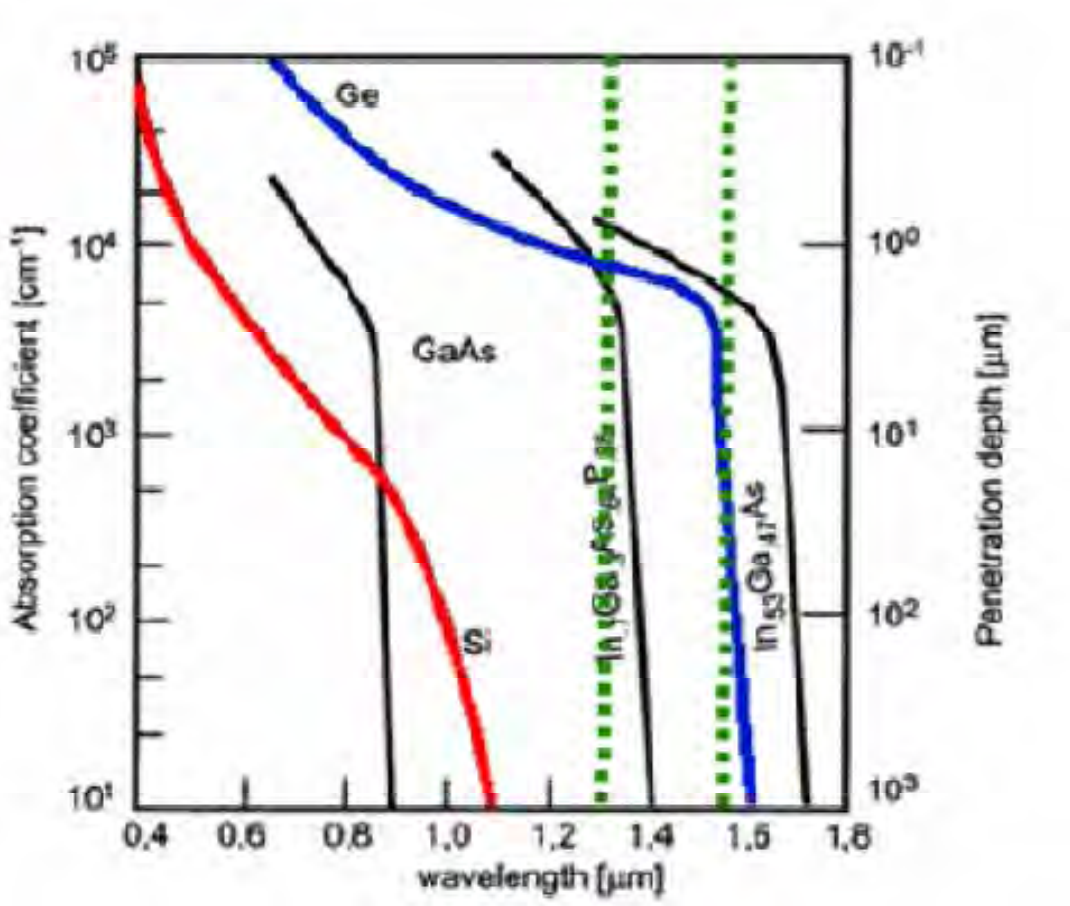


**Fig4.7:**Absorption coefficient and penetration depth of various materials as a function of λ. Green lines mark important communications wavelengths of 1.31μm and 1.55μm[75].

The current design for a silicon based photo detector is to have a layer of SiGe between a P-type and an N-type layer. Because of the electric field across the SiGe layer (induced by the p-i-n structure) electrons raised to the conduction band by photon absorption will generate a current. A very desirable property of silicon is that it makes for great APDs (Avalanche Photo Detector) in which an electron pushed to the conduction band will set off a chain reaction in which many electrons will be affected causing a greater current spike to occur. Electrical probes can then be connected to the P and N regions of the photo-detector to transfer the data to the logic portion of the chip.

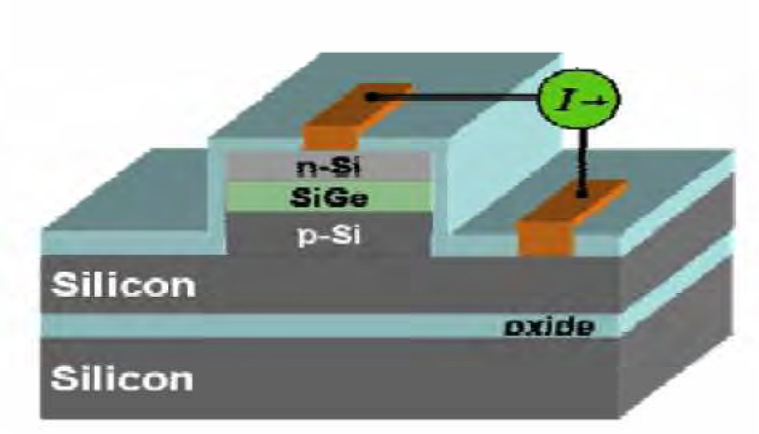


**Fig 4.8:** SiGe waveguide-based photo-detector on a SOI wafer[75].

Technical concerns facing the silicon photo-detector include responsivity, speed, and dark current limitations. The speed of this device must match up with the speed of the modulator or else data imposed on the optical connection will be lost. The responsivity is an important factor in the design of the detector because determines whether or not an signal will produce enough of a voltage boost to be interpreted as a 1 as opposed to a 0. Dark current is a major aspect concerning the performance of the detector. Dark current is caused by lattice miss matches and creates a current which is present even when light is not. If the dark current of a photo-detector is too high the detector will read a 1 when it should be reading 0. Another major problem caused by dark current is that it degrades the quality of an incoming optical signal by making the voltage difference between a 1 and a 0 significantly smaller.

Silicon nanocristal is not only applicable for photonic, in the next chapter we will see application of silicon nanocristals for light emitting devices ,memory devices and for solar cell.

# Chapter 5

# Application of silicon nanocrystals for light emitting devices memory devices and solar cells

In this unit we have going to see the application of silicon nanocristallites for light emitting devices, memory device and solar cells.

## 5.1 Light Emitting Devices Based on Si-Nanoclusters

The implementation of efficient optical functions in Si would greatly simplify the integration of electronic and photonic devices. The first goal is to fabricate efficient and electrically-driven room temperature light emission sources in Si. For application in the telecommunication field emission at 1.54 μm is requested. This target has been pursued by Si-nc embedded in $SiO_2$ prepared by thermal annealing of SiOx films synthesized by PECVD can be successfully used to fabricate light emitting MOS devices. The EMMI image of a device with a Si content of 46 at.% and annealed at 1100°C is reported in Fig. 5.2a. The image reveals an intense emission, very stable and almost homogeneous over the whole active *area*. The bright emission we observe starts at a voltage of −15 V, with a current density of the order of about 90 $\mu A/cm^2$

A spectral analysis of the light emitted from the devices has been performed by EL measurements. Fig. 5.2b shows the room temperature EL spectrum measured in a device with a Si content of 42 at.% in the SiOx layer. The spectrum was measured by biasing the device with a square pulse at a frequency of 55 Hz with a voltage of −48 V. It is therefore straightforward to attribute the EL signal to electron-hole pair recombination in the Si-nc dispersed in the oxide layer. Devices based on Si-nc are very stable and can work continuously for several days without deterioration. The estimated internal efficiency is about 1%.

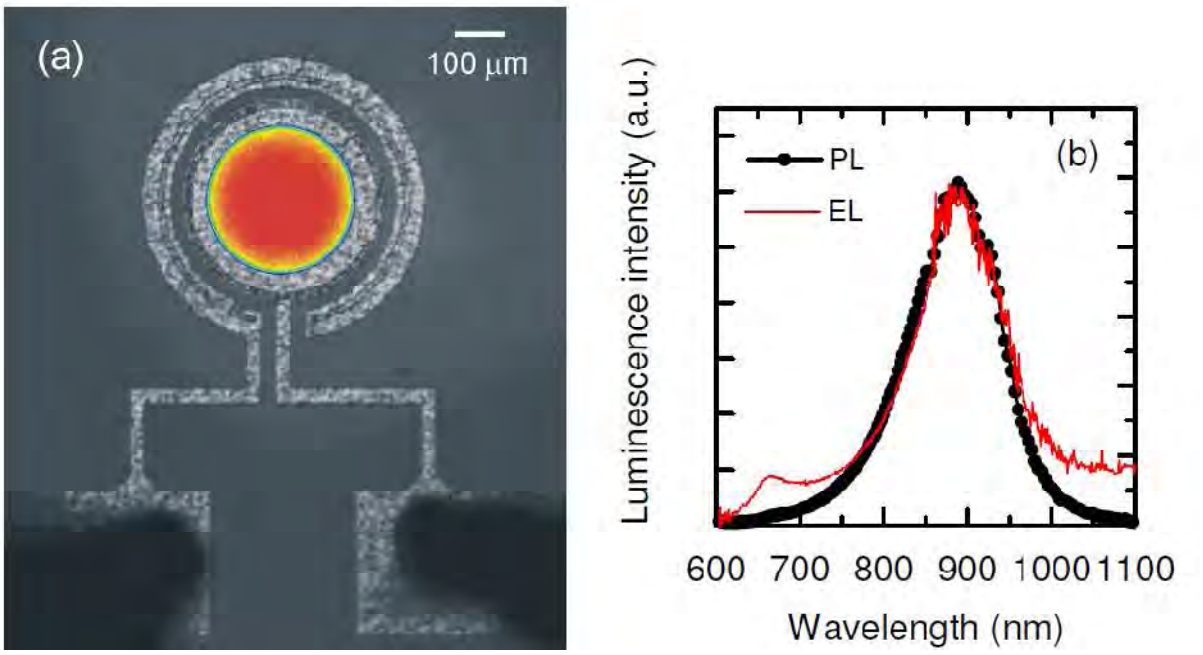


**Fig. 5.1:** (a) EMMI image of a device with 46 at.% Si annealed at 1100°C for 1 h. The colors indicate different intensities of the emitted light, red being the highest. (b)Comparison between the PL and the EL spectra of a device with a Si content of 42 at.% in the SiOx layer. The EL spectrum was measured with a voltage of −48 V and a current density of 4 mA/cm$^2$.

Amorphous Si nanoclusters may constitute an interesting alternative to Si-nc for the fabrication of light emitting devices to be used for the monolithic integration of optical and electrical functions in Si VLSI technology. In fact, they exhibit an intense room temperature EL in the same range of wavelengths already found for their crystalline counterpart, with the advantage to be formed at a temperature of 900°C, while, as above discussed, at least 1100°C are needed for the formation of Si-nc.[37,38].

### 5.1.1 Enhancement of the efficiency of light emitting devices based on Si nanoclusters by coupling with photonic crystals

The external efficiency of devices based on Si nanostructures can be considerably enhanced by the integration with a two dimensional photonic crystal, thus paving the way to a whole new class of practical Si light emitters. A proper design of the photonic crystal is able to extract a large amount of light, which would be otherwise wasted, thus enhancing the overall efficiency by over a factor of four. In fact, in a typical Si LED, as a result of the high refractive index of Si ($n$ = 3.5), most of the emitted light remains trapped inside the device by total internal reflection, thus severely limiting the overall performance. The realization of a two-dimensional photonic crystal on the device surface was proposed to overcome this limitation, and proved its effectiveness within an optically pumped III-V quantum well embedded in a multilayer microcavity[39].

In order to better explore this phenomenon we have performed EL measurements on photonic crystal, random and unpatterned devices. The EL data reported in Fig. 5.5a were taken under a −20 V forward bias and at a current density of 22 A/cm$^2$. The unpatterned device shows an EL emission characterised by two peaks at around 750 nm and 1000 nm. As previously discussed, the EL from amorphous Si nanoclusters is similar to the nc counterpart. The peculiar shape of the spectrum shown in Fig. 5.5a cannot be considered an intrinsic characteristic of the amorphous clusters but the result of interferences occurring within the polysilicon layer.

The enhancement achieved accounts for more than a factor of four. We hence characterized the EL intensity of the photonic crystal device as a function of observation angle. This feature is particularly evident in Fig. 5.5b, which is the experimental polar distribution of the emitted radiation at 860 nm taken by tilting the device along the GM direction. It is interesting to note that the radiation pattern of the photonic crystal device is extremely directional, once more demonstrating the presence of diffraction effects.

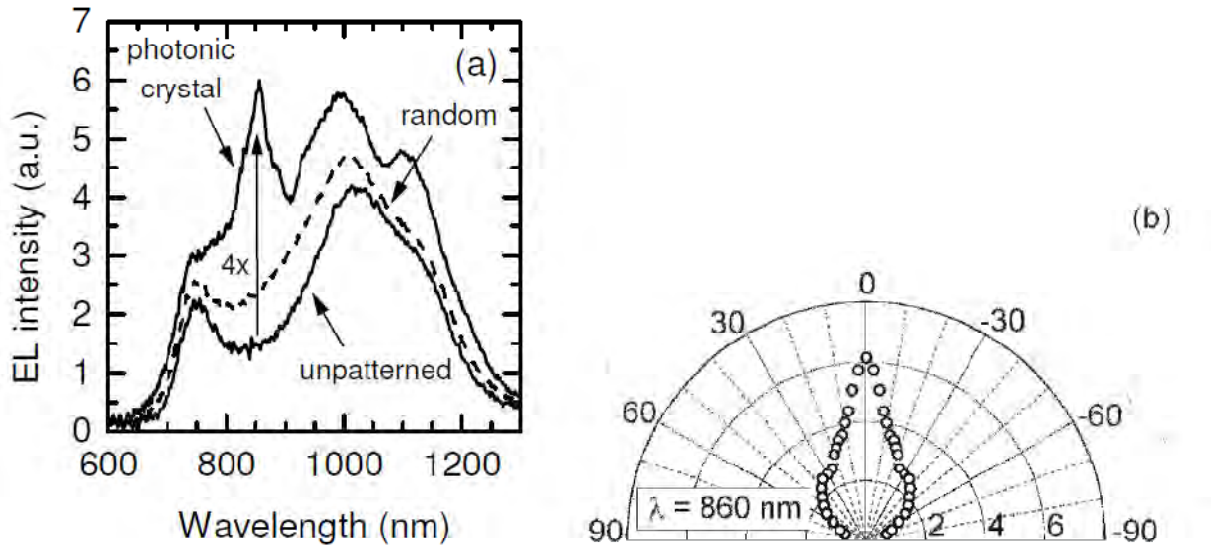


**Fig. 5.2:** (a) EL spectra for the unpatterned, random, and photonic crystal devices. An EL intensity enhancement accounting for a factor of 4 at 860 nm is demonstrated in the photonic crystal device. (b) Polar distribution of the emitted radiation at a wavelength of 860 nm. Tilt is along GM direction.

## 5.2 Silicon nanocrystal for dot memory

Nonvolatile memory devices using nc-Si-dot-based electrically isolated charge-storage nodes in an oxide film as a floating gate have emerged in the last decade [50], where charge leakages through localized oxide defects could be greatly reduced, therefore, improving performance reliabilities as well as the memory-retention time. Furthermore, a much thinner tunneling oxide film in nanodot memory devices causes a major tunneling mechanism due to direct tunneling hence enabling a faster write/erase speed compared to Fowler–Nordheim tunneling which is met in conventional flash type memory devices. Charge injection and storage in dense arrays of nc-Si dots in $SiO_2$ is a key aspect of their performance.

The ultimate goal for this class of devices is approaching the few- or single-electron storage in a small number of nc-Si elements at room temperature, relying on the Coulomb blockade effects as a new electron transport principle, commonly referred to as single electron memory. The high-density integration capability and low-power consumption enable them to be an attractive candidate for the next generation digital nonvolatile memory applications. However, in spite of the successful demonstrations of memory operations based on single-electron transports, the

charge retention time of nc- Si dot memory devices is too short for practical nonvolatile memory applications [51]. The improved retention time was demonstrated to be possible without any significant loss of programming speed based on the modifications of floating-gates by the dual memory nodes [52].

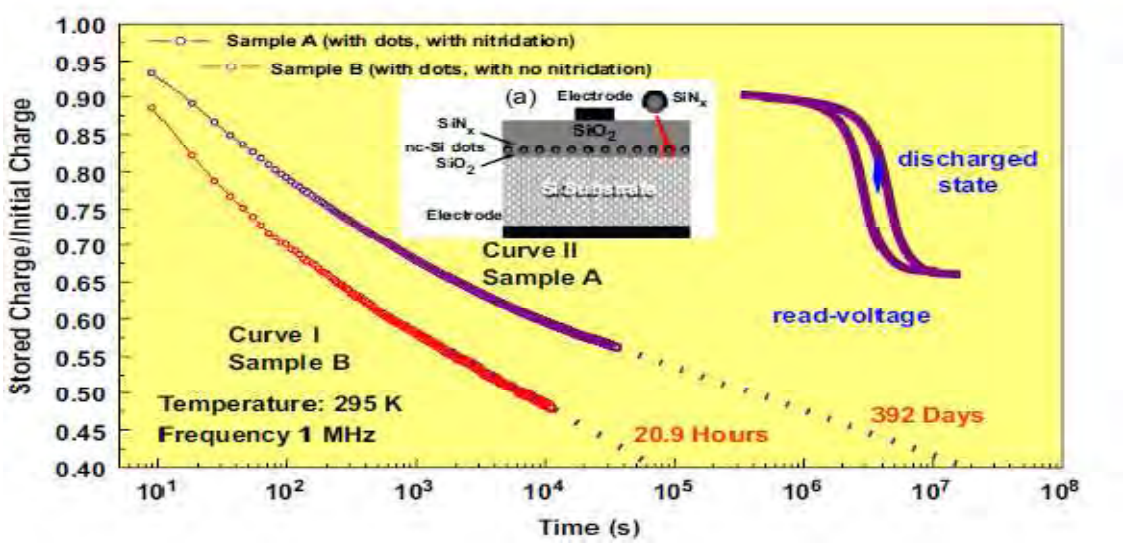


**Figure 5.3:** Time dependence of the stored-charge from the flat-band state, after electrons were injected in floating-gates, shows a logarithmic discharging behavior. The gate voltage was kept at the initial flat-band voltage: -1.6V for sample A (surface nitrided nc-Si dots) and -2.4V for sample B (without nitridation). The inset shows the structure of memory device.

Charge retention characteristics reveal how charges are stored in nc-Si memory nodes. A major essential issue for nc-Si memory devices in nonvolatile memory applications is the data retention characteristics over extended period of time. After some electrons are trapped, at a chosen reading voltage (e.g., flat-band voltage), the stored electrons have a finite probability to tunnel back to the drain, which could cause a gradual shift of channel current or capacitance of SiO2/nc–Si/SiO2 diode. These gradual shifts reflect barrier heights/widths, internal electric fields, defect or interfacial states, and so on. Therefore, investigations of time dependences of memory windows as well as charging/discharging behaviors of nc-Si dots correlated with Coulomb blockade and quantum confinement effects offer better understanding of charge retention characteristics of nc-Si memory devices [53].

Investigation of charging and discharging in nc-Si dots, based on measurements of capacitance–voltage and conductance–voltage characteristics, shows that interface states and deep defects correspond to charging and discharging processes. However, at low defect and interfacial state density, electron charge/discharge is only dominated by bounding electrons in nc-Si dots.

For a $SiO_2$/nc–Si/$SiO_2$ capacitor memory device, in time-dependent capacitance measurements, the memory-retention time was found to exceed 5 h (calculated time for the loss of about 10% of the original charge) at room temperature. Instead of being governed by deep defects, at low defect and interfacial state density, electron charge/discharge is only dominated by electron bounded in nc-Si dots. A repulsive ‘‘built-in’’ electric field from nc-Si dots to silicon substrate created and controlled by charge loss in nc-Si dots was proposed to explain such long-term retention time [54]. On the other hand, a longer retention time can be achieved by introducing a certain number of deep trapping centers in nc-Si dots with decreasing the interfacial states at the tunneling-oxide/Si interface. Compared with pure nc-Si floating-gate memory devices, nitrided nc-Si-dot-based memory devices were experimentally demonstrated to be helpful to remarkably increase retention time by three orders of magnitude, as shown in Fig 5.3, without sacrificing write/erase time, in which memory operations based on combined charge/discharge processes of nitrided nc-Si dot systems. The stored charges in such memory nodes were identified not only in nc-Si dots but also in defect-states of silicon-nitride films, corresponding to electron delocalized and localized states, respectively.

## 5.3 Silicon nanoclusters for solar cell

Nanocrystalline silicon films have recently attracted attention for use in photovoltaic solar cells since they show promise for providing an approach that results in lower cost and higher efficiency than conventional solar cells [17, 18, 19]. Traditionally, most of the commercially available solar cells are made out of various forms of silicon wafers.

Single crystalline silicon solar cells provide relatively good efficiencies, however they suffer from high cost. In addition, crystalline silicon has low absorption coefficient and narrower band gap than that desired for solar cell applications. Solar light with energy much larger than the bandgap, when absorbed by the material is converted into heat rather than electricity thus

reducing the efficiency. Polycrystalline silicon or amorphous silicon solar cells are available at lower cost; however their conversion efficiency is lower than their single crystalline counterparts. In addition, amorphous silicon shows photodegradation and reduced stability under long-term illumination. The use of nanocrystalline silicon holds the promise to realize both high performance and low cost in photovoltaic solar cells. Nanoscale silicon provides much better chemical stability than thin film polycrystalline or amorphous silicon under long-term operation.

Its wider bandgap is much more suitable for solar cell applications than the narrow indirect bandgap of single crystalline silicon. Furthermore, silicon nanostructuring may provide the means for achieving a bandgap-engineered material to be used in tandem solar cells. Silicon nanoparticles of appropriate sizes or superlattices of $Si/SiO_2$, Si/SiGe and/or Si/C can be integrated with other materials with appropriate bandgap, such as amorphous silicon, polycrystalline silicon, or single crystalline silicon, to manufacture stacked solar cells. These types of solar cells can provide a variation of the effective bandgap across the material, allowing a significant portion of the solar spectrum to be efficiently coupled into the device and produce electricity.

### 5.3.1 Using silicon nanostructures for the improvement of silicon solarcells' efficiency

Silicon nanostructures (ns-Si) show interesting optical and electrical properties as a result of the band gap widening caused by quantum confinement effects. Along with their potential utilization for silicon-based light emitters' fabrication, they could also represent an appealing option for the improvement of energy conversion efficiency in silicon-based solar cells whether by using their luminescence properties (photon down-conversion) or the excess photocurrent produced by an improved high-energy photon's absorption.

In this work, we present on the luminescence and absorption studies of non-stoichiometric silica (SiOx) and silicon nitride (SiNx) layers containing silicon nanostructures (ns-Si) in view of their application for silicon solar cell's efficiency improvement. The photoluminescence emission (PL) shows a rather high efficiency in both kind of layers and was found to be only a factor 100 below that of highly luminescent porous silicon (pi-Si) samples.

Silicon-rich silica layers (x =1.5) were fabricated by low pressure chemical vapor deposition (LPCVD) on a 63-nm-thick $SiO_2$ layer previously grown by thermal oxidation onto a silicon substrate. The silicon excess was introduced by adjusting the $N_2O/SiH_4$ gas flow ratio and the conditions were controlled to obtain a 200-nm-thick SiOx film. After deposition, the $Si/SiO_2$ phase separation was assured by an annealing step in $N_2$ at 1000 $^0$C during 30 min. A final annealing step was performed at 1000 $^0$C during 30–120 min under $O_2$ atmosphere to synthesize and passivate the ns-Si. On the other hand, silicon-rich silicon nitride layers (SiNx) were fabricated by photo-assisted chemical vapour deposition (UVCVD) of 15-nm-thick layers on previously oxidized silicon substrates.

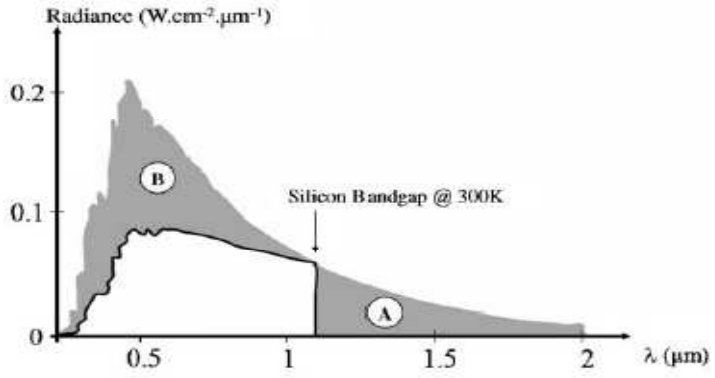


**Figure 5.4:** Energy loss processes in a solar cell schematically depicted. The zone denoted by A represents the low-energy photon losses resulting from the material band gap, whereas the zone denoted by B represents the high-energy photon losses resulting from phonon scattering (thermalization).

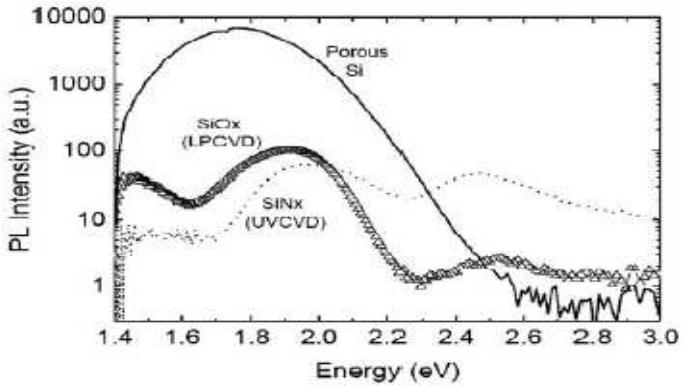


**Figure 5.5:** Comparison of PL spectra between porous silicon, SiNx and SiOx samples. The PL intensity of SiNx and SiOx samples is equivalent but still a factor 100 below that of porous silicon sample[76].

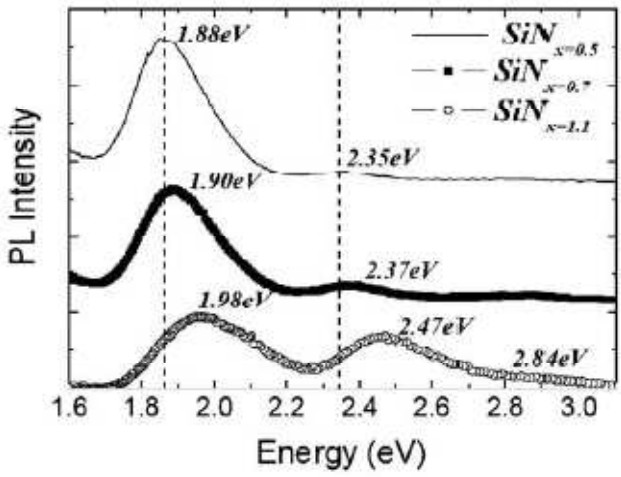


**Figure 5.6:** PL spectrum obtained from SiNx= samples for 0.5<x <1.1 showing the energy dependence of the emission on silicon content [76].

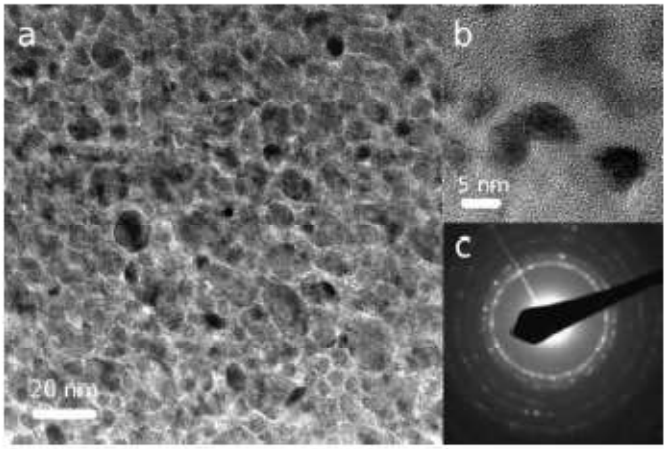


**Figure 5.7** HRTEM image of nanocrystalline Si precipitates embedded in a UV assisted silicon-rich (x =1.1) nitride film: (a) observation of the Si precipitates on a large scale with a density of $1.5 \times 10^{12}$ $cm^{-2}$; (b) zoom image showing the shape and length of few Si nanocrystals; and (c) ring patterns for the transmission electron diffraction from the Si nanoprecipitates showing their crystalline nature [76].

Figure 5.5 shows the photoluminescence spectra obtained from silicon-rich samples (SiOx=1.5 and SiNx=0.7) compared to the PL signal of the pi-Si sample.The PL intensity of the SiNx samples was found to be equivalent to that of the SiOx samples and both of them about 100 times weaker than that observed on pi-Si samples. The important point here is that the SiNx layers have been deposited at low substrate's temperature (Ts<75 $^{o}$C) and no postdeposition

annealing treatment was required whereas for the SiOx samples a high temperature annealing has been performed in order to obtain the PL signal. The PL spectrum of the SiNx=0.5 sample shown in Figure 5.6 has two PL bands located at 1.88eV and 2.35eV. These bands show a blue shift along with an emerging of a very weak intensity third PL band at 2.84 eV when the stoichiometry of the layer is changed from SiNx=0.5 to SiNx=1.1. This PL energy dependence with silicon content can be explained either by a change of the band gap of the SiN layer [33, 34] or by an exciton quantum confinement within silicon nanostructures imbedded in the layer [35 , 36].

The first assumption considers that the SiN band gap increases with N content due to the replacement of Si–Si bonds located at the top of the valence band by Si–N bonds, which are deeper valence band states, causing the displacement of the bottom of the conduction band as a result of the substitution of Si–Si antibonding states by Si–N antibonding ones. On the other hand, the second assumption proposes an exciton confinement within ns-Si surrounded by SiN barriers and, when the N content in the layer increases, it would cause an increase of the barriers' height and therefore an enhancement of confinement effects on excitons leading to the band gap increase. In our case, the TEM measurements performed in the SiN layers (see in Figure. 5.7) clearly demonstrate the existence of crystalline

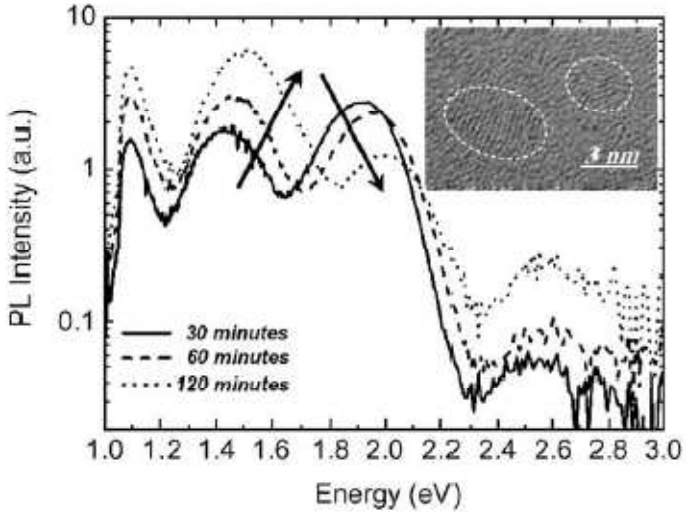


**Figure 5.8:** PL dependence on annealing duration under $O_2$ atmosphere for SiOx=1.5 samples. An increase of annealing temperature reduces the nanoparticle size producing an increase of the optical band gap and a blue shift of the PL energy.Inset: Typical TEM image showing the silicon nanostructures formed after high temperature annealing [76].

# Chapter 6
# Summary and future outlook

## 6.1 summary

Bulk silicon is poor emitter of light, while silicon nanostructures (porous silicon, quantum dots, quantum wells and nanoclusters), exhibit strong photoluminescence at room temperature which is observed only after a drastic reduction of silicon size and has been related to quantum confinement effect. Quantum confinement effect widens the band gap that occurs when the nanostructures size become comparable to the Bohr exciton radius in bulk silicon.

Silicon nanocristals have tremendous applications in the photoluminescence, optoelectronic and photonic devices. They can be easily integrated into silicon wafer processing and utilized for biological, chemical, optical sensors and memory devices.

It has been discussed that silicon nanostructures can be fabricated by different methods. The most common ones are electrochemical iodization of bulk silicon in an HF electrolyte, plasma enhanced chemical vapor deposition (PECVD), ion-implantation.

We have seen The Pseudo-Potential-Density Functional Theory Applied to Nanostructures. These first principles pseudo-potentials often relay on density functional theories, which are exact in principle but in practice relay on various approximations such as the local density approximation [33]. Its purpose is to preview how to implement this approximation method in nanostructures such as that of silicon.

We have concluded that quantum confinement effects and surface passivation increase the optical absorption coefficient and dielectric function of the nano-silicon with decreasing size of the nanocluster. Therefore, the photoluminescence intensity increase with decreasing size of the nanocluster for silicon nanocluster whose effective size (6-10nm) as observed by many experiment are in conformity with our work. Optical properties of nano-silicon is affected by

quantum confinement effect.Quantum confinement effect change the indirect band gap nature of bulk silicon to direct band gap in the nano-silicon whose average size is below and equal to 10nm. Although quantum confinement alone cannot explain the whole physics of silicon nanostructures but gives explanation of the observation of luminescence.

Silicon Photonics is just now becoming a reality and has the potential to be tomorrow's method of data interconnects. Research is steadily developing this vision and is showing many positive results. With the development of the silicon modulator and silicon laser more people are shedding their skepticism of silicon as an optical material and beginning to find ways to implement this revolutionary technology. With every improvement come a new set of relationships and a new set of questions. The process of optimizing these optical circuits and refining their production will provide research opportunities for many years to come.

Nanocrystalline silicon films have recently attracted attention for use in photovoltaic solar cells since they show promise for providing an approach that results in lower cost and higher efficiency than conventional solar cells**.**The results of the optical and morphological characterization of SiNx and SiOx layers have been shown in view of their application for solar cell efficiency improvement. The PL signal has an equivalent intensity for both kind of layer but it remains a factor ¨100 below that of porous silicon samples. In addition, the PC spectroscopy has revealed an excess photocurrent at high-energy excitation (blue-UV) in both layers. This signal has been related to absorption within ns-Si and could be used to improve the blue-UV response in ‘‘classical’’ solar cells. Finally, the main asset of this material is the low cost of implementation, as a simple modification of the antireflection coating layer (ARC) during the deposition step would allow obtaining the silicon nanoparticles.

## 6.2 Future Outlook

Understanding how size and surface effects change optical and electronic property of nano structures is a key step in nanoscinece. Experimentalists and quantum simulation experts are working together to establish a basic knowledge of the structured and optical properties of semiconductor nanostructures. Some day a scientist will know exactly how to produce a nano

widget to detect a deadly pathogen. Perhaps the widget must emit blue light, and the scientist will know that using a nano particle of a given size and density produces the desired wavelength.

Nanotechnology is expected to have an impact on nearly every industry. The research community is actively perusing hundreds of applications in nanomaterials, nano electronics and bionanotechnology. Nanodevices and nanoelectronics will have applications in medical treatments and diagnostics, faster, computers and in sensors. Although progress in integrable Si-based detectors and wave guides is very encouraging, electro luminescent devices have still some way to go to meet the requirement of quantum efficiency, high operating frequency and life time necessary to compete with the hybrid solution using III-V optoelectronic systems.

The quantum dot will be the basic component of future quantum computing elements in the future and expectations are very large for emergence of new ”noncontinuous” technology based on the quantum dot technology. The vision of nanophotonics which are optical functionality:on the smallest possible size scale, on the lowest possible energy level and on the shortest possible timescale

There is a strong need for the development of photovoltaic cells with low cost, high efficiency, and good stability. In thin film technologies, there exists a common problem with conversion efficiency due to poor materials quality; the photogenerated electrons and holes cannot travel very far before recombination (short free-carrier diffusion lengths) and are hence lost for power conversion. If the solar cell can be made using nanoscale heterojunctions, then every photogenerated carrier will have less distance to travel, and the problem of recombination can be greatly reduced .Developing Quantum dots for photovoltaic solar cell is the future out look.Silicon nanocrystals with novel functions such as charge and energy quantization and efficient photon/electron emission are promising for future electronics applications. Silicon nanodot memory device can be a promising alternative for high-density nonvolatile memory.

# Bibliography

[1] Lorenzo Pavesi. Monograph on Photonics Applications of Nanosilicon,Universita di Trento-Italy, 2005.

[2] www.micronova.fi/units/epg/publications/publications2001/Reports**25**.pdf.

[3] S. Veprek. Thin Solid films **297,** 145-153(1997).

[4] Url: http:||sience.unitn.it/~semicon/(December 2009).

[5] http://jrc.cem.umn.edu.(December 2009).

[6] Using silicon to understand silicon: Doping of Nanostructures, James R. Chlikowsky, The electronic society interface, spring 2005.

[7] http://jrc.cems.umn.edu/(November 2009).

[8] Optical excitations in Nanostructures: Application of Time Dependent Density Functional Theory to Sin (n= 3-10), Igor Vasiliev, Serder Ogut, and R. Chelikowsky.

[9] http://www.meliorum.com(December 2009).

[10] Quantum dots: phenomenology, photonic and electronic properties Modeling and technology, Frederic Boxberg and Jukka and Tulkki.

[11] http://www.webelements.com (December 2009).

[12] http://www.webelements.com (December 2009).

[13] Nanocrystals: “Keeping pace with Moor’s law,” Arne Nylandsted and BrianBech Nielson.

[14] The Optical properties of silicon nanocrystals and the role of hydrogen pasivation, A.R.Wilkinson.

[15] Silicon Nanostructures For photonics, L.Pavesi, P.Bettoti, M.Cazzanelli, S.Cella, N.Daldosso L.Dal Negro, B.Danese, Z.Gaburro.

[16] Electrical properties of silicon nanocrystals embedded in an ultra thin oxide, Nanothecnology **10** 127-131(1999).

[17] D. Song, E. Cho, G. Conibeer, Y. Huang, and M. A. Green, Appl. Phys. Lett. **9** (12) 123510 (2007).

[18] H. Kawauchi, M. Isomura, T. Matsui, M. Kondo, Journal of Non-Crystalline Solids, **354** pp. 2109 – 2112 (2008).

[19] D. Song, E. Cho, G. Conibeer, C. Flynn, Y. Huang, M. A. Green, Solar energy Materials and Solar Cells **(92)** pp. 474 – 481 (2008).

[20] S. Limaye, S. Subramanian, B. Goller, J. Diener, and D. Kovalev, Phys. Stat.Sol. **(a) 204**,1297 (2007).

[21] S. Botti, M. L. Terranova, V. Sessa, S. Piccirillo and M. Rossi, Appl.Organometal. Chem. **15**, 388 (2001).

[22] M. Ehbrecht, B. Kohn, F. Huisken, M. A. Laguna, V. Paillard, Phys. Rev. **B 56**, 6958 (1997).

[23] C. Delerue, G. Allan, M. Lannoo, Phys. Rev. **B 48**, 11024 (1993).

[24] P. Bettotti, M. Cazzanelli, L. Dal Negro, B. Danese, Z. Gaburro, C. J. Oton, G. Vijaya Prakash and L. Pavesi, J. Phys,: Condens. Matter **14**, 8253 (2002).

[25] X. Badel in Electrochemically etched pore arrays in silicon for X-ray imaging detectors, Ph.D. thesis, KTH, Stockholm, Sweden, 2005.

[26] Tae-Youb Kim, Nae-Man Park, Kyung-Hyun Kim, Young-Woo Ok, Tae-Yeon Seong, Cheo- Jong Choi and Gun Yong Sung, Mat. Res. Soc. Symp. Proc. Vol. **817**, 78 (2004).

[27] S. Schuppler et al, Phys. Rev. Lett. **72**, 2648 (1994).

[28] T. van Buuren, L. N. Dinh, L. L. Chase, W. J. Siekhaus, and L. J. Terminello, Phys. Rev. Lett. **80**, 3803 (1998).

[29] A. Puzder, A. J. Williamson, J. C. Grossman, and G. Galli, Phys. Rev. Lett. **88**,97401 (2002).

[30] J. I. Pankove, Optical Processes in Semiconductors, Prentice-Hall, Englewood Cliffs, New Jersey, 1971.

[31] Karl W. B¨oer, Survey of Semiconductor Physics: Electrons and Other Particles in Bulk Semiconductors, Nostrand Reinhold, 1990.

[32] Jasprit Singh: www.eecs.umich.edu/_singh, John-Wiley, 2001.

[33] S. Hasegawa, M. Matuura, Y. Kurata, Appl. Phys. Lett. **49** ,1272(1986).

[34] J.F. Justo, F. de Brito Mota, A. Fazzio, Phys. Rev., B **65,** 073202(2002).

[35] V.A. Gritsenko, K.S. Zhuravlev, A.D. Milov, et al., Thin Solid Films **353** 20 (1999).

[36] N.M. Park, C.J. Choi, T.Y. Seong, et al., Phys. Rev. Lett. **86** ,1355 (2001).

[37] A. Irrera, F. Iacona, I. Crupi, C. D. Presti, G. Franzò, C. Bongiorno, D. Sanfilippo,G. Di Stefano, A. Piana, P. G. Fallica, A. Canino and F. Priolo, *Nanotechnology* **17**,1428 (2006).

[38] F. Iacona, A. Irrera, G. Franzò, D. Pacifici, I. Crupi, M. Miritello, C. D. Presti andF. Priolo, *IEEE J. Sel. Top.Quantum Electron.* **12**, 1596 (2006).

[39] A. Erchak, D. J. Ripin, S. Fan, P. Rakich, J. D. Joannopoulos, E. P. Ippen, G. S.Petrich and L. A. Kolodziejski, *Appl. Phys. Lett.* **78**, 563 (2001).

[40] A. G. Cullis, L. T. Canham and P. D. J. Calcott, *J. Appl. Phys.* **82**, 909 (1997).

[41] D. Kovalev, H. Heckler, G. Polisski and F. Koch, *Phys. Stat. Sol. (a)* **215**, 871(1999).

[42] J. Heitmann, F. Müller, M. Zacharias and U. Gösele, *Adv. Mater.* **17**, 795 (2005).

[43] M. S. Hybertsen, *Phys. Rev. Lett.* **72**, 1514 (1994); M. S. Hybertsen in "*Porous Silicon Science and Technology*" Ed. by J.-C.Vial and J. Derrien, Springer (1995)]. *in Silicon Nanocrystals Assemblies* 423.

[44] D. Kovalev, M. Ben-Chorin, J. Diener, B. Averboukh, G. Polisski and F. Koch, *Phys. Rev. Lett.* **79**, 119 (1997).

[45] K. J. Nash, P. D. J. Calcott, L. T. Canham and R. J. Needs, *Phys. Rev.* **B51**, 17698 (1995).

[46] J. Diener, D. Kovalev, G. Polisski, H. Heckler and F. Koch, *Phys. Stat. Sol.* **(b) 214**,R13 (1999).

[47] R. J. Walters, J. Kalkman, A. Polman, H. A. Atwater and M. J. A. de Dood, *Phys.Rev.* **B73**, 132302- 1 (2006).

[48] Sychugov, R. Juhasz, J. Valenta and J. Linnros, *Phys. Rev. Lett.* **94**, 087405 (2005); I. Sychugov, R. Juhasz, J. Valenta, A. Zhang, P. Pirouz and J. Linnros, *Appl. Surf. Science* **252**, 5249 (2006).

[49] C. Delerue, M. Lanoo, G. Allan, E. Martin, I. Mihalcescu, J. C. Vial, R. Romestain, F. Muller and A. Bsiesy, *Phys. Rev. Lett.* **75**, 2228 (1995).

[50] J.J. Welser, S. Tiwari, S. Rishton, K.Y. Lee, Y. Lee, IEEE Electron.Devices Lett. **18**, 278(1997).

[51] B.J. Hinds, T. Yamanaka, S. Oda, J. Appl. Phys. **90** (12), 6402(2001).

[52] S. Huang, K. Arai, K. Usami, S. Oda, IEEE Trans. Nanotechnol. **3,** 210 (2004).

[53] S. Huang, R.T. Tung, S. Oda, J. Appl. Phys. **94 ,**7261(2003).

[54] S. Huang, S. Banerjee, R.T. Tung, S. Oda, J. Appl. Phys. **93** ,7261(2003).

[55] D. E. Woon and T. H. Dunning Jr, *J. Chem. Phys.* **98**, 1358–1371 (1993).

[56] A. Polman in Silicon-based Photonics, European Materials Research Society Meeting 2006, Nice, France; M. Fujii et al., Appl. Phys. Lett. **71**,1198 (1997).

[57] Tadesse Tenaw Kassa, silicon nanostructures,a Graduate Project submitted to the scool of graduate study of Addis Ababa university,27(2006).

[58] Wondwosen Tilahun Metaferia, verification of multiple mechanism model for the Photoluminescence of oxidized porous silicon and nanosilicon particle embedded in silicon Oxide A Thesis Submitted to the School of Graduate Studies of Addis Ababa University, 27(2006).

[59] Tadesse Tenaw Kassa, silicon nanostructures,a Graduate Project submitted to the scool of graduate study of Addis Ababa university,51(2006).

[60] Tadesse Tenaw Kassa, silicon nanostructures,a Graduate Project submitted to the scool of graduate study of Addis Ababa university,52(2006).

[61] Tadesse Tenaw Kassa, silicon nanostructures,a Graduate Project submitted to the scool of graduate study of Addis Ababa university,53(2006).

[62] Tadesse Tenaw Kassa, silicon nanostructures,a Graduate Project submitted to the scool of graduate study of Addis Ababa university,52(2006).

[63] Hagos Gebrehiwet, absorption coefficient and dielectric function of direct band gap silicon nanocrystallites A thesis submitted to the School of Graduate Studies Addis Ababa University, 22(2007).

[64] Wondwosen Tilahun Metaferia, verification of multiple mechanism model for the photoluminescence of oxidized porous silicon and nanosilicon particle embedded in silicon oxide A Thesis Submitted to the School of Graduate Studies of Addis Ababa University, 9(2006).

[67] Tadesse Tenaw Kassa, silicon nanostructures,a Graduate Project submitted to the scool of graduate study of Addis Ababa university,43(2006).

[68] Tadesse Tenaw Kassa, silicon nanostructures,a Graduate Project submitted to the scool of graduate study of Addis Ababa university,44(2006).

[69] Tadesse Tenaw Kassa, silicon nanostructures,a Graduate Project submitted to the scool of graduate study of Addis Ababa university,45(2006).

[70] Tadesse Tenaw Kassa, silicon nanostructures,a Graduate Project submitted to the scool of graduate study of Addis Ababa university,46(2006).

[71] Tadesse Tenaw Kassa, silicon nanostructures,a Graduate Project submitted to the scool of graduate study of Addis Ababa university,55(2006).

[72] Tadesse Tenaw Kassa, silicon nanostructures,a Graduate Project submitted to the scool of graduate study of Addis Ababa university,60(2006).

[73] Tadesse Tenaw Kassa, silicon nanostructures,a Graduate Project submitted to the scool of graduate study of Addis Ababa university,62(2006).

[74] Tadesse Tenaw Kassa, silicon nanostructures,a Graduate Project submitted to the scool of graduate study of Addis Ababa university,63(2006).

[75] Michael R. Bynum, Silicon Photonics, Winter 2006.

[ 76] J. De la Torre , G. Bremond , M. Lemiti , G. Guillot , P. Mur , N. Buffet, Thin Solid Films 511 – 512 (2006).